HHS Public Access

Author manuscript

Mol Cell. Author manuscript; available in PMC 2019 March 15.

Published in final edited form as:

Mol Cell. 2018 March 15; 69(6): 938–952.e6. doi:10.1016/j.molcel.2018.02.018.

CDK and MAPK synergistically regulate signaling dynamics via a shared multi-site phosphorylation region on the scaffold protein Ste5

María Victoria Repetto[1,2], **Matthew J. Winters**[3], **Alan Bush**[1,2], **Wolfgang Reiter**[4], **David Maria Hollenstein**[4], **Gustav Ammerer**[4], **Peter M. Pryciak**[3,*], and **Alejandro Colman-Lerner**[1,2,5,*]

[1]Universidad de Buenos Aires (UBA), Facultad de Ciencias Exactas y Naturales, Departamento de Fisiología, Biología Molecular y Celular, Buenos Aires, Argentina

[2]CONICET-UBA, Instituto de Fisiología, Biología Molecular y Neurociencias (IFIBYNE), Buenos Aires, C1428EHA, Argentina

[3]Department of Biochemistry and Molecular Pharmacology, University of Massachusetts Medical School, Worcester, MA 01605, USA

[4]Department for Biochemistry, Max F. Perutz Laboratories, University of Vienna, Vienna, A-1030, Austria

Summary

We report an unanticipated system of joint regulation by CDK and MAPK, involving collaborative multi-site phosphorylation of a single substrate. In budding yeast, the protein Ste5 controls signaling through a G1 arrest pathway. Upon cell cycle entry, CDK inhibits Ste5 via multiple phosphorylation sites, disrupting its membrane association. Using quantitative time-lapse microscopy, we examined Ste5 membrane recruitment dynamics at different cell cycle stages. Surprisingly, in S-phase, where Ste5 recruitment should be blocked, we observed an initial recruitment followed by a steep drop-off. This delayed inhibition revealed a requirement for both CDK activity and negative feedback from the pathway MAPK Fus3. Mutagenesis, mass spectrometry, and electrophoretic analyses suggest that the CDK and MAPK modify shared sites, which are most extensively phosphorylated when both kinases are active and able to bind their

[*]Correspondence: peter.pryciak@umassmed.edu (PMP), colman-lerner@fbmc.fcen.uba.ar (ACL).
[5]Lead Contact

Supplemental Information

Supplemental Information includes seven figures and four tables.

Author Contributions

ACL and PMP designed the project. MVR performed quantitative microscopy experiments and affiliated analyses, with assistance from AB. MJW made Ste5 mutations and yeast strains, and performed signaling and Ste5-NT phosphorylation assays. WR, DMH, and GA performed mass spectrometry experiments and analysis. PMP, ACL, and MVR analyzed data and prepared the manuscript.

Declaration of Interests

The authors declare no competing interests.

docking sites on Ste5. Such collaborative phosphorylation can broaden regulatory inputs and diversify output dynamics of signaling pathways.

Graphical abstract

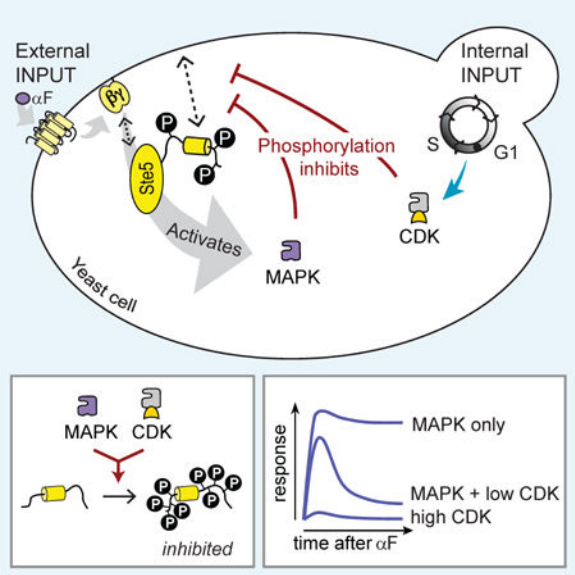

Introduction

Normal cell behavior depends on the ability to detect and respond to extracellular signals. Such responses commonly begin at the plasma membrane, and then spread throughout the cell by signal transduction pathways. Importantly, the potential responses to a stimulus must be integrated with other information about the physiological state of the cell. For example, in the yeast *S. cerevisiae*, mating pheromones trigger a signaling pathway in a manner that depends on cell cycle position. The current study probes the mechanism of this regulatory circuit, which involves two regulatory networks found in all eukaryotes: a mitogen-activated protein kinase (MAPK) cascade and cyclin dependent kinases (CDKs).

Response to yeast pheromones involves the dynamic assembly of a membrane-localized signaling complex (Bardwell, 2005; Alvaro and Thorner, 2016). Signaling begins when pheromones secreted by haploid cells of one mating type bind to G protein-coupled receptors on the plasma membrane of cells of the opposite mating type. Activated Gβγ dimers then turn on a MAPK cascade via membrane recruitment of a scaffold protein, Ste5, which binds both Gβγ and the pathway kinases. The MAPK then stimulates downstream responses (Figure 1A).

The pheromone pathway has a mutually antagonistic relationship with the cell cycle: MAPK signaling promotes arrest of the cell cycle in G1 phase, whereas this signaling is inhibited in late G1 when cells pass the cell cycle commitment step known as “Start” (Hartwell et al., 1974). Early work showed that pheromone response is inhibited by CDK in complex with the late G1 cyclins Cln1/2 (Oehlen and Cross, 1994), and later studies revealed that the

inhibited step is membrane recruitment of Ste5 (Strickfaden et al., 2007). Specifically, the target is a membranebinding domain in Ste5, dubbed the PM domain for its role in plasma membrane localization, in which it acts together with Gβγ binding (Winters et al., 2005) (Figure 1B). When cells transition from G1 to S, the ability of this PM domain to bind to the plasma membrane is countered by CDK phosphorylation of eight flanking sites. If these sites are mutated to non-phosphorylatable residues, pheromone signaling is not inhibited during the cell cycle (Strickfaden et al., 2007).

Two further aspects of this regulation are relevant to the new findings in this study. First, effective inhibition of Ste5 requires phosphorylation at multiple sites. That is, when varying numbers of sites were mutated, the degree of inhibition became gradually stronger as more sites were available (Strickfaden et al., 2007), revealing a regulatory continuum in which incomplete phosphorylation yields partial inhibition. Second, efficient CDK phosphorylation of Ste5 requires a new class of cyclin docking motif, recognized specifically by the G1/S cyclins Cln1 and Cln2 (Bhaduri and Pryciak, 2011; Koivomagi et al., 2011). These “LP motifs” (named for their enrichment in Leu and Pro residues) are found in a variety of Cln1/2-CDK substrates. The specificity of the Ste5 LP motif for Cln1/2 helps explain why pheromone signaling is blocked only in early post-Start stages and not later when S- and M-phase CDKs are active.

This work describes a surprising new facet of this regulation that was revealed by recent advances in quantitative microscopy, in which the redistribution of Ste5 from cytoplasm to membrane can be assayed in a timeframe of seconds to minutes (Yu et al., 2008; Bush and Colman-Lerner, 2013). These previous studies monitored the average behavior in asynchronous cell populations. Notably, after the initial recruitment of Ste5 to the membrane there was a mild detachment, which was not observed if the pathway’s MAPK, Fus3, was inhibited (Yu et al., 2008). Such findings established that a negative feedback loop from the MAPK dampens Ste5 recruitment, by reducing the effective binding affinity between Ste5 and Gβγ (Bush and Colman-Lerner, 2013), although it remained unknown if the direct target was Ste5 itself, the G protein, and/or another factor (Figure 1C). Here, we report that cell cycle regulation and this feedback use the same phosphorylation sites in Ste5, and that CDK and MAPK activities can jointly contribute to enhance the multi-site phosphorylation of a shared substrate. This collaborative effect may be especially helpful at cell cycle stages when the key cyclins are not at peak levels.

Results

Single-cell recruitment assays reveal cell cycle stage-specific dynamics

Previous studies on Ste5 recruitment dynamics measured the average behavior in asynchronous populations (Yu et al., 2008; Bush and Colman-Lerner, 2013). Here, we monitored individual cells, in which Ste5 was tagged with three tandem YFPs (*STE5-YFPx3*; driven by its native promoter). We observed extensive variability in Ste5 recruitment (Figure 1D). To dissect the effects of cell cycle position, we classified cells by stage, focusing on G1 (pre-Start), post-Start and S-phase cells. This classification used as a diagnostic marker either morphology (i.e., budding status before and after pheromone stimulation) or localization of the repressor Whi5 (fused to mKO_{kappa}), which exits the

nucleus at Start (Doncic et al., 2011) (Figures 1E, S1A-B). We expected two behavioral groups: recruiting cells (G1) and nonrecruiting cells (post-Start and S-phase), depending on whether Cln1/2 is expressed. Both groups were indeed present, but, surprisingly, there was a third behavior: many post-Start and S-phase cells exhibited an initial peak followed by a strong decline (Figures 1F, S1B). This “peak and decline” behavior revealed that the full manifestation of the cell cycle effect was not evident immediately but instead developed over the first 5–6 minutes of pheromone stimulation, enough time to activate the downstream MAPK. I.e., it suggested a dependence on both cell cycle position and negative feedback from the pathway.

A Principal Component Analysis revealed that cell-to-cell variability was explained primarily by two variables: initial recruitment and the degree of subsequent decline (Figure 1G-H, see Method Details). In general, in pre-Start cells, initial Ste5 recruitment was greatest and the decline was mildest. In post-Start cells, initial recruitment was affected minimally but the decline increased substantially such that it often exceeded 50% of the initial recruitment value (Figure 1H). By S phase, initial recruitment was strongly reduced (Figure 1H), in some cases to levels indistinguishable from untreated cells. Based on these results, we defined threshold criteria that distinguish most G1 cells from post-Start and S phase cells (Figure 1G-H, dashed lines), and used them to categorize each cell into one of three dynamic behaviors (Figure 1I); this categorization facilitated comparison of numerous mutants and experimental perturbations described below. We observed similar behaviors regardless of the number of *STE5-YFPx3* copies integrated (Figure S1C-D), and over a range of pheromone doses (Figure S1E-G). To validate interpretations, we applied statistical tests (see Method Details) to data from all recruitment experiments (see Table S1). Overall, we interpret the different behaviors to reflect a combination of the increasing concentration of Cln1/2 as cells pass Start, plus a time-dependent response to pheromone. This combined effect of cell cycle position and response time led us to suspect a concerted action of CDK and MAPK.

CDK and MAPK activities both contribute to regulation of Ste5 recruitment

To constrain models for these complex recruitment dynamics, we first tested the role of the PM domain, the target of cell cycle regulation (Strickfaden et al., 2007). The PM domain (Figure 2A) overlaps a nuclear localization signal (NLS), and so we used mutations that disrupt one or both targeting functions (Winters et al., 2005). Initial recruitment was abolished if the PM domain was deleted (ΔPM), or if it harbored point mutations that disrupt membrane binding (PM^*_{memb}; Figure 2B). These results showed that the PM domain is essential at the earliest stages of recruitment, ruling out the possibility that the initial phase is CDK-resistant because the PM domain is not yet required. Recruitment dynamics were normal with PM domain mutations that only disrupt nuclear localization (PM^*_{nuc}; Figure 2B), arguing against a role for Ste5 nuclear shuttling in the cell cycle regulation. Note that in these and all subsequent experiments, we restricted our analysis to G1 and S cells, given that the post-Start behaviors were intermediate.

Next, we tested a mutant in which the 8 N-terminal phosphorylation sites flanking the PM domain were absent, Ste5-8A (Figure 2A) (Strickfaden et al., 2007). As expected for a

mutant lacking CDK sites, initial recruitment was not inhibited in S phase. Surprisingly, however, the decline behavior was also disrupted (i.e., < 50% in most cells; Figure 2C). This joint disruption of both stage- and time-dependent effects revealed a close interdependence between the cell cycle regulation and negative feedback. Indeed, by using analog-sensitive alleles of either the CDK (*cdc28-as2*) or the MAPK (*fus3-as2)* (Bishop et al., 2000; Colman-Lerner et al., 2005; Yu et al., 2008), we observed that both kinase activities were essential for the decline behavior in S phase (Figures 2D and S2A). (In *cdc28-as2* strains, an apparent residual decline in S-phase cells reflected a measurement artifact caused by redistribution of Ste5 to the small bud, which lies outside the cell contour defined by the Cell-ID software; Figure S2B.) It is noteworthy that inhibiting Fus3 often yielded a subtle "incline" behavior (i.e., a slow increase in recruitment after the initial peak), implying mild negative feedback in G1 (see Discussion). Findings from drugsensitive strains were supported by similar results in Δ*fus3* cells or in cells lacking Cln1 and Cln2 (Figure 2E). Unlike Fus3, the alternate MAPK Kss1 did not affect recruitment (Figure S2C). Finally, by conducting long time-lapse recordings in mutant strains that fail to arrest in G1 after stimulation with pheromone, we found that Ste5 was displaced from the membrane during the G1/S transition, and that this required Fus3 (Figure S2D). The need for Fus3 activity in these cell cycle effects indicated a direct role for the MAPK, ruling out simple scenarios in which CDK alone regulates Ste5 but only after its membrane recruitment.

CDK and MAPK co-regulate the same target domain in Ste5

To explain why full inhibition of Ste5 membrane localization requires both CDK and MAPK activities, we considered two models (Figure 3A). In the "different target" model, CDK and MAPK phosphorylate either different proteins or different sites in the same protein. Each set of phosphorylations alone partially reduces the net membrane affinity of Ste5, but both sets must occur simultaneously to fully displace Ste5. In the "shared target" model, CDK and MAPK promote phosphorylation of the same sites, which is conceivable as they recognize the same core motif (SP or TP) (Pinna and Ruzzene, 1996). Here, the number of sites phosphorylated depends on the combined level of Cln1/2-CDK and MAPK activities; e.g., maximal phosphorylation might be achieved either by peak levels of Cln1/2-CDK alone or by intermediate levels of both Cln1/2-CDK and MAPK together (Figure 3B).

Several observations argued against the first model and favored the second, "shared target" model. First, recruitment was essentially blocked (and the need for Fus3 bypassed) by mimicking phosphorylation at the 8 N-terminal sites, using a Ste5-16E allele (Strickfaden et al., 2007) that has each of the 8 SP/TP motifs replaced with two glutamates (EE) to fully mimic the charges of 8 phosphorylations (Figure 3C). This result suggested that full phosphorylation at these 8 sites is sufficient to prevent recruitment, and hence there is no strict necessity for other proteins or sites to be phosphorylated. Because initial recruitment is not blocked in many WT S-phase cells, we suspected that in such cells these sites were incompletely phosphorylated before pheromone stimulation and then became fully phosphorylated in the decline phase. Second, we used a Ste5-8E mutant, which also lacks the 8 N-terminal sites but mimics only half of the charges gained by phosphorylation (Strickfaden et al., 2007). The resulting partial inhibition of the PM domain should sensitize this mutant to further inhibitory effects elsewhere, yet it showed almost no decline behavior

and practically no effect of removing Fus3 (Fig. 3D). This insensitivity to Fus3 strongly argues against the hypothesis that Fus3 acts on a distinct target. Third, recruitment behavior was unaffected in mutants in which Fus3 was unable to act on alternative targets (Gpa1, Ste4, Far1 and Sst2) (Figure S3A-B). Fourth, expressing *CLN2* from a strong promoter (P_{GAL1}) showed that high levels of Cln2-CDK activity alone could block initial recruitment (Figure 3E). This effect was not triggered by S- or M-phase cyclins (*CLB5* or *CLB2*, respectively) (Figure S3C), in agreement with the cyclin specificity seen for phosphorylation of Ste5 (Strickfaden et al., 2007; Bhaduri and Pryciak, 2011) and Fus3 (Figure S3D). Consistent with the capacity for CDK to block recruitment on its own, P_{GAL1}-*CLN2* also bypassed the requirement for Fus3 (Figure 3E); notably, however, for the fraction of cells in which recruitment was not fully blocked, the remaining decline required Fus3 (Figure 3E). Altogether, these results suggest that phosphorylation of the Ste5 N-terminus can suffice to explain the observed behaviors, and that the CDK and MAPK co-regulate this domain.

Cln1/2-CDK activity levels dictate inhibition severity and MAPK dependence

The preceding results suggested that, at sufficiently high levels, Cln2-CDK activity can drive full (or nearly full) blockade of initial recruitment. Hence, peak and decline behavior might occur when cells have only intermediate levels of Cln2-CDK activity, such that the full blockade requires assistance from the MAPK. To test this view, we directly varied Cln2-CDK activity by expressing P_{GAL1}-*CLN2* in cells with an inhibitable CDK (*cdc28-as2*), and then varying the inhibitor concentration. In one set of experiments we monitored Ste5 recruitment. As CDK activity increased (i.e., decreasing inhibitor), peak recruitment gradually decreased to negligible levels (Figure 3F, top, and Figure S3E-F); removing Fus3 did not alter the initial recruitment but it eliminated the decline phase. These results argue that initial recruitment is controlled by CDK alone, which make sense as Fus3 activity is minimal before pheromone stimulation, but that Fus3 is essential for the subsequent decline. In related experiments, we assayed Fus3 phosphorylation (Figure 3F, bottom). Again, when varying the CDK inhibitor, we observed that the highest levels of Cln2-CDK activity could strongly block initial signaling, but intermediate levels showed a peak and decline response that suggested additional inhibition via negative feedback. Similarly, when we assayed Fus3 phosphorylation kinetics in synchronous cultures, the initial activation was most strongly blocked when Cln2 levels were highest, whereas a transient peak and decline response was seen when Cln2 levels were lower or when Cdc28 activity was partially inhibited (Figures 3G, S3G-H). Finally, we also modulated Cln2-CDK activity by varying the copy number of an integrated P_{MET3}-*CLN2* cassette. Here, the ability of Cln2-CDK to block signaling was partly reversed by inhibiting Fus3, but mainly at lower (2x) dosage of P_{MET3}-*CLN2* and not at higher (3x) dosage (Figure S3I). Collectively, these findings show that the Cln2-CDK activity level dictates both the severity of Ste5 inhibition and the reliance on Fus3.

If cells with intermediate levels of Cln2-CDK activity cannot fully inhibit Ste5 recruitment until pheromone activates the MAPK, then pre-activating the MAPK should eliminate the need for initial recruitment. To test this idea, we induced MAPK activity with a P_{GAL1}-*STE11*Δ*N-STE7* construct (Strickfaden and Pryciak, 2008), which encodes a MAPKKK-MAPKK fusion protein that activates Fus3 in the absence of pheromone (Figure 3H). This pre-activation of Fus3 greatly reduced initial recruitment in S phase, such that most cells

showed no recruitment (Figure 3I-J); this argues that the normal delay before the decline onset in S-phase cells indeed reflects the need to activate Fus3. In G1 cells, however, pre-activation of Fus3 did not block recruitment, indicating that its effects in S-phase cells require coaction with Cln1/2-CDK. This contrasts with the ability of high Cln2-CDK activity alone to block recruitment. It is unclear if this contrast reflects a quantitative difference in kinase activity (of CDK vs. Fus3), or a qualitative difference (e.g., distinct site preferences or capacities for processive phosphorylation). Nevertheless, it is clear that activation of Fus3 by normal or ectopic routes cannot strongly block recruitment in G1 cells.

CDK and MAPK collaborate to maximize multi-site phosphorylation of Ste5

To obtain independent evidence that the CDK and MAPK have a collaborative effect on Ste5 phosphorylation, we used a gel migration assay. Detection of phosphorylation-induced mobility shifts was enhanced by using an N-terminal fragment of Ste5 (Ste5-NT; expressed in *STE5-WT* cells), which harbors twelve SP/TP sites plus docking motifs for the cyclin (Cln1/2) and MAPK (Fus3) (Figure 4A). We monitored Ste5-NT mobility after release from an M-phase arrest, with and without a brief (5 minute) pheromone treatment. We saw mobility shifts triggered by pheromone in G1 (i.e., before Cln2 appeared), or without pheromone treatment in S phase (after Cln2 appeared), but the most extensive shift occurred in the combined condition: S phase cells plus pheromone (Figure 4B-C). This joint effect occurred regardless of the Ste5 fragment length (Figure S4A) or the gene dosage of full-length *STE5* (Figure S4B), and was confirmed to reflect phosphorylation by phosphatase treatment in vitro (Figure S4C). It also required the 8 N-terminal sites (Figure 4C), as well as both CDK and Fus3 activities, but not Kss1 (Figures 4D, S4D); the shifts were reversed rapidly (5–10 minutes) by inhibiting either CDK or Fus3 (Figure S4E), indicating continuous antagonism by counteracting phosphatases. The role of other Ste5 sequence motifs will be reported in subsequent sections. (Note that pheromone triggers some phosphorylation independent of both Fus3 and SP/TP sites (Figure S4F), possibly due to an upstream kinase such as Ste11 or Ste7.) Overall, these results show that CDK and MAPK activity cooperate to drive maximal phosphorylation of Ste5.

Remarkably, although Fus3 activation was inhibited in S phase cells, there was enough activity to contribute to the combined phosphorylation (Figure 4B-C), in accord with our findings that Fus3 helps inhibit Ste5 recruitment in S phase. Furthermore, even though the average concentration of activated Fus3 was low, a local high concentration might exist at signaling sites enriched in pathway kinases (Maeder et al., 2007). Indeed, Ste5-NT phosphorylation induced by pheromone (but not cell cycle entry) was disrupted by the mutation C180A (Figure S4G), which blocks binding of this fragment to Gβγ (Inouye et al., 1997; Feng et al., 1998; Winters et al., 2005), thus preventing its translocation to sites where active Fus3 is generated (via the endogenous Ste5). Thus, the finding that joint phosphorylation of Ste5 occurs despite low Fus3 activity helps explain how negative feedback from Fus3 can antagonize Ste5 recruitment in S phase.

Pheromone signaling and cell cycle entry promote phosphorylation of shared sites

The preceding results raised the question of whether the CDK and the MAPK share sites. Whereas the eight N-terminal sites in Ste5 are important for cell cycle regulation

(Strickfaden et al., 2007), the four central sites were thought to be phosphorylated by the MAPK (Bhattacharyya et al., 2006; Malleshaiah et al., 2010). Yet, all of these are minimal SP/TP sites, lacking optimal sequence context for either kinase. Therefore, we analyzed Ste5 phosphorylation by quantitative mass spectrometry, using synchronous cultures to test two conditions: the effect of pheromone in G1 and the effect of cell cycle entry (G1 vs. S, without pheromone). Changes in both phosphorylated and unphosphorylated Ste5 peptides were measured by label-free quantification. The results uncovered a remarkably large number of phosphorylated residues: 66 were detected in total, and 27 showed reproducibly quantifiable changes (Figures 4E-F and S5; Table S2; and Table M3 associated with PRIDE dataset PDX006154). These include most of the 15 SP/TP sites in Ste5, plus many non-SP/TP sites. Multiple phospho-accepting residues often resided in the same tryptic peptide, resulting in differently phosphorylated variants that could hamper unambiguous interpretation of the modification behavior at individual sites. Thus, we also compared overall phosphorylation patterns by sorting peptides into “phosphoislands” (Langella et al., 2017); i.e., sequence regions with one or more phosphorylation sites on overlapping peptides, plus their unphosphorylated counterparts (Figures 4F and S5). This process defines sets of juxtaposed sites that are assessed jointly. Importantly, the overall phosphorylation of each region can be determined by the change in abundance of the unphosphorylated counter peptide(s). Remarkably, we observed little distinction in the sequences phosphorylated in response to pheromone (in G1) versus in response to cell cycle entry (without pheromone), including N-terminal regions near the PM domain as well as central regions near the Cln2 and Fus3 docking motifs. These regions were extensively phosphorylated, as the reduction in unphosphorylated peptides often exceeded 2-fold, indicating that the majority of Ste5 molecules were modified. Thus, in broad overview, the CDK and the MAPK promote phosphorylation of largely shared sites, including those previously implicated in distinct regulatory circuits.

Despite the extensive overlap, some differences were notable. First, some regions were phosphorylated preferentially in response to pheromone (namely, phosphoislands 6, 9, 12, 13, 16, and 18); hence, as described below, we probed sites within these regions (i.e., S167, T371, T456, S577, and S684). Second, we noticed some subtle biases when comparing phosphorylation across all sites in the two stimulatory conditions (Figures 4G and S5C). Relative to pheromone, phosphorylation promoted by cell cycle entry was slightly biased toward the N-terminal sites, and against TP sites, favoring SP sites instead. The latter might arise either from a mild preference of the CDK for SP (Suzuki et al., 2015) or from phosphatases that prefer phospho-TP (Godfrey et al., 2017) being more active in S phase than in G1. If such a bias was compensated by the MAPK, this could create synergy between MAPK and CDK, and a version of this concept will be addressed in a later section.

Given the multiplicity of sites and the likely complexity of their phosphorylation (see Discussion), efforts to dissect preferences of individual kinases in vitro were left for later studies. Here, we focused on determining which sites contribute to the *in vivo* behaviors. We observed no notable effects on Ste5 recruitment by mutating a site near the Gβγ-binding domain (S167N) or any of several sites in the C-terminal half (SP/TP and non-SP/TP) (Figure S6B). Interestingly, several non-SP/TP sites were clustered near the eight regulatory SP/TP sites in the N-terminus, suggesting they might help regulate the PM domain. Thus,

we created a mutant lacking nine non-SP/TP sites (n9AN; Figure 5A). Unlike the 8A mutant, the n9AN mutant did not prevent P_{GAL1}-*CLN2* from inhibiting signaling (Figure 5B), indicating that these non-SP/TP sites are not absolutely required for regulation by Cln2-CDK. However, in recruitment assays, the n9AN mutant showed a partial loss of the S-phase decline behavior, such that most cells showed declines of less than 50% (Figure 5C-D). Hence, when Cln2-CDK activity is sub-maximal, these additional N-terminal sites may facilitate acquisition of enough phosphates to inhibit Ste5 recruitment.

MAPK control of Ste5 recruitment is separable from the central phosphorylation sites

Prior studies suggested that the four central SP/TP sites in Ste5 are targeted by Fus3 (Malleshaiah et al., 2010); indeed, in our mass spectrometry analysis, three of these four sites showed pheromone-induced phosphorylation (Figure 4E). To ask if they help control Ste5 recruitment, we first tested if their phosphorylation was sufficient to explain the role of Fus3, by using a phospho-mimetic 4E mutant (i.e., four Ser/Thr residues replaced with Glu). The 4E phenotypes were essentially indistinguishable from WT: both the S-phase specific decline behavior and the collaborative phosphorylation were unchanged, and each phenotype still required Fus3 and the 8 N-terminal phosphorylation sites (Figure 5E-F). As a further control, we tested a non-phosphorylatable 4Q mutant (i.e., Ser/Thr replaced with uncharged Gln residues), and found that it resembled the WT and 4E alleles (Figure 5E-F). These results rule out the hypothesis that the only role for Fus3 is to phosphorylate these four central SP/TP sites. Instead, even when those sites cannot be modified, Fus3 can still regulate Ste5 recruitment and phosphorylation, and this role of Fus3 involves the 8 N-terminal sites. A simple explanation is that Fus3 can phosphorylate sites in either region, which is supported by mass spectrometry (Figure 4E) and by additional Ste5-NT mobility shift data showing that Fus3 can drive modification of each region independently, even in G1 cells (Figure S6C).

Regulatory roles for kinase docking sequences

Next, we probed the role of docking sites on Ste5 for the cyclin and the MAPK, known as the LP site (Bhaduri and Pryciak, 2011; Koivomagi et al., 2011) and the D site (Bhattacharyya et al., 2006), respectively (Figure 6A). In Ste5-NT phosphorylation assays, mutation of each site caused a specific defect consistent with its predicted function. Namely, the LP site mutation (llpp) disrupted phosphorylation in response to cell cycle entry but not in response to pheromone, whereas the D site mutation (ND) had the reverse effect; moreover, either mutation prevented the maximum phosphorylation (Figure 6B). (Note, in these assays the mutations were only in the Ste5-NT fragment, not in full-length Ste5 that activates Fus3.) Also, when the LP motif was disrupted, the extent of pheromone-induced shift was reduced in S-phase, reflecting the reduced activation of Fus3 in this phase (Figure 6B); the contrast with the WT fragment starkly illustrates how this weak Fus3-dependent phosphorylation enhances the LP motif-dependent action of Cln1/2-CDK.

In Ste5 recruitment assays, cell cycle regulation was most disrupted when both docking sites were mutated simultaneously (Figure 6C). Notably, the single mutants affected distinct aspects (Figure 6C, S7A). With the D site mutated, initial recruitment was still reduced in S phase, but the decline was eliminated, suggesting that partial inhibition initiated by the CDK

could not be enhanced further by the MAPK. Mutating the LP site had a converse pattern: initial recruitment was not lower in S phase cells, and they lacked the class of cells showing no recruitment, but there was a decline, as if the activated MAPK partly compensated for the Cln1/2 docking defect. With both sites mutated (llpp + ND), the phenotype was the sum of the individual defects: high initial recruitment and lack of decline in S phase. Similarly, when we assayed Fus3 phosphorylation in S phase (Figure 6D), the single mutants showed partial defects in inhibition, and the double mutant showed a near complete defect comparable to Ste5-8A. Thus, consistent with the roles for each kinase, each docking site contributes distinctly to the cell cycle phenotype. We also analyzed early signaling kinetics in cells that constitutively express Cln2 (P_{GAL1}-*CLN2*) (Figure 6E). This blocked initial signaling in cells with WT Ste5, but when the LP site was mutated signaling peaked and then declined, and this decline required an intact D site. If the LP site was intact, the D site was not needed for the effect of P_{GAL1}-*CLN2*. Again, these results suggested that when Cln2-CDK phosphorylation of Ste5 is sub-maximal, Fus3 can compensate, and hence that the need for Fus3 depends on the effective potency of Cln2-CDK. Moreover, when using the Ste5-8E mutant to partially mimic phosphorylation, there was reduced signaling but no decline phase (Figure 6E), supporting earlier recruitment results (Figure 3D) to suggest that negative feedback occurs via these sites.

MAPK might serve a priming function for processive CDK phosphorylation

Collaborative phosphorylation could occur via a simple additive mechanism or via a priming mechanism, in which phosphorylation by one kinase makes the other more effective. CDK substrates can be primed by prior phosphorylation at threonine residues; these phospho-Thr sites bind the Cks1 subunit of the CDK complex (Figure 6F, *inset*) to promote processive phosphorylation of multi-site substrates (Koivomagi et al., 2013; McGrath et al., 2013). Hence, we wondered if MAPK phosphorylation of Thr residues in the Ste5 N-terminus could serve a priming role that helps Cln1/2-CDK-Cks1 phosphorylate the remaining sites to completion. Three of the eight SP/TP sites in the Ste5 N-terminus are TP sites (Figure 6F). When these were changed to SP sites (creating the 8SP mutant), the S-phase decline was reduced to less than 50% in most cells (Figure 6G-H). In gel mobility shift assays, the 8SP mutation primarily reduced phosphorylation by CDK rather than MAPK, and it prevented the collaborative production of maximally shifted forms (Figure 6I). Thus, the TP sites do indeed allow low MAPK activity to promote full CDK-dependent phosphorylation. Reliance on the MAPK could be accentuated if the CDK disfavors TP sites, as our mass spectrometry results suggest. Additive and priming mechanisms are not mutually exclusive, which might explain why the 8SP mutant defect is incomplete.

The 8SP and WT forms of Ste5-NT showed illuminating differences in mobility behavior. With the WT fragment, the CDK-induced shift was bimodal (Figure S7B), implying a divided population of Ste5 molecules, phosphorylated on either a few or many sites. A bimodal pattern could arise from Cks1-dependent processivity, if molecules that acquire phospho-Thr are quickly converted to a highly phosphorylated state while those that acquire only phospho-Ser remain lightly modified. If so, any MAPK-induced increase in Thr phosphorylation could shift the distribution in favor of highly phosphorylated forms. Indeed, with the 8SP mutant the CDK-induced shift appeared more unimodal (Figure S7B). Also,

for 8SP the shift induced by pheromone in S phase was reduced compared to that in G1 (Figures 6I and S7B); this was reminiscent of the pattern noted earlier for mutations in the LP motif (Figure 6B), and thus fits the view that processivity is enhanced by both Cks1 and cyclin docking (Koivomagi et al., 2013). These phenotypes suggest that future advances in phospho-isoform identification can foster detailed insights into the mechanisms of collaborative phosphorylation.

Discussion

This study reveals an unexpected overlap between two regulatory phenomena, previously considered separate. The scaffold protein Ste5 was known to be negatively regulated both by CDK activity during the cell cycle and by negative feedback from the pathway MAPK, but we find that these two regulatory pathways are related. In particular, we show that the previous observations of negative feedback in asynchronous populations, in which Fus3 triggered a mild decline in membrane-localized Ste5 (Yu et al., 2008; Bush and Colman-Lerner, 2013), actually reflect the average behavior of two distinct phenotypic classes: cells with strong declines, and cells with minor declines. We also show that the cell cycle regulation of Ste5 membrane localization depends on negative feedback from Fus3. The net findings indicate that cell cycle regulation and negative feedback operate via the same sites, and that the CDK and MAPK can jointly contribute to complete phosphorylation (Figure 7A). This arrangement provides regulatory diversity such that signaling can be either mildly tuned or more strongly blocked, depending on the cell cycle stage and kinase activities present (Figure 7B). Moreover, the MAPK feedback can compensate for low Cln1/2 levels. This cooperative regulation broadens the inhibitory window to include times shortly after passing Start (Figure 7C), when Cln1/2 are just beginning to be expressed (Doncic et al., 2011).

The regulatory behaviors revealed here also help explain other recent findings on signaling in this pathway. Specifically, in studies that monitored Fus3 activity in single cells, using either FRET-based or translocation-based sensors, post-Start cells showed a transient period of weak signaling before returning to a prolonged inhibitory phase (Durandau et al., 2015; Conlon et al., 2016). Our findings indicate that this brief response reflects a transient recruitment of Ste5 in cells that have not yet reached peak Cln1/2-CDK activity.

If this regulatory system mainly serves to inhibit pheromone response as cells pass Start, it would seem simplest to depend solely on Cln1/2-CDK. Is there an advantage to involving Fus3? Inhibiting Fus3 often caused a subtle “incline” behavior in G1, implying that Fus3 mildly dampens Ste5 localization even in G1-arrested, mating cells, which lack CDK activity. This negative feedback could yield partial phosphorylation that mildly tempers Ste5 membrane affinity, such that it is not fully inhibited but is more responsive to changes in stimulus strength or distribution. In this scenario, the MAPK-mediated inhibition serves a CDK-independent tuning function, and then the CDK-mediated regulation provides a further layer of control so that the combined effect yields full inhibition.

A generalized form of this regulatory module could add flexibility to other pathways. The combination of a negative feedback loop (NFBL) with variable inhibition (VIN) generates a

range of behaviors (Figure 7D). A NFBL alone cannot shut off its upstream signaling completely, but it can quicken the response (Alon, 2006) and adjust output strength (Yu et al., 2008). At the other extreme, a strong VIN alone can shut off signaling. In between, the circuit yields an adjustable transient response that is sharply inactivated after a brief delay (Figure 7D). The time delay could allow cells to retain memory of past signal exposure. In fact, yeast cells can store (and transmit to the next generation) information of past pheromone exposure, by accumulating cytoplasmic Far1 (Doncic et al., 2015).

Presumably, many CDK targets do not require input from another kinase. Hence those that do might be intrinsically inefficient CDK substrates, due to the number, distribution, or sequence context of phospho-acceptor sites, or the affinity of cyclin docking motifs, etc. Evolutionary variation of these features could then tune the degree to which CDK regulates a given substrate independently versus concertedly. Collaborative regulation can also involve different forms of CDK. For example, multi-site phosphorylation of yeast Sic1 is initiated by Cln1/2-Cdk1 but then finished by Clb5-Cdk1 (Koivomagi et al., 2011); such regulatory relays can ensure that outcomes have both precise timing and rapid execution (Yang et al., 2013).

Our mass spectrometry and mobility shift data provide clear evidence for Fus3-dependent phosphorylation of Ste5 in vivo. In each assay, pheromone triggered phosphorylation of the majority of Ste5 molecules. These findings do not support prior claims, based on indirect evidence, that Ste5 phosphorylation is reduced by strong pheromone stimulation (Malleshaiah et al., 2010). It is possible, however, that membrane and cytoplasmic pools of Ste5 are phosphorylated differently, which is not captured in bulk assays. Curiously, activation of Fus3 by pheromone or by P_{GAL1}-*STE11*Δ*N*-*STE7* does not lead to a full blockade of Ste5 recruitment, in contrast to P_{GAL1}-*CLN2*. This might be due to more stringent site preferences, such that Fus3 poorly phosphorylates some N-terminal sites, or Fus3 might not be sufficiently processive to convert Ste5 molecules to the fully phosphorylated form. Processive cyclin-CDK complexes might be intrinsically more capable of fully inhibiting Ste5, but depend on the MAPK when at sub-peak expression levels. Thus, our results suggest a hierarchy, in which Cln1/2-CDK is essential for full inhibition and capable of near complete inhibition alone (if sufficiently active), whereas Fus3 alone is capable of only mild dampening but can assist the CDK in full inhibition.

Due to the large number of sites we identified in Ste5, including both SP/TP and non-SP/TP types, the routes by which maximal multi-site phosphorylation is promoted by collaborating enzymes are likely to be complex. Full understanding will require extensive work to identify any preferred “initial” sites and how they alter subsequent phosphorylation. Recent studies of Sic1 (Koivomagi et al., 2011) exemplify how full multi-site phosphorylation can involve more than one kinase, due to site biases, positions of docking motifs, priming phosphorylation, and Cks1-mediated processivity. Until similar efforts are extended to additional substrates, however, it will remain unclear which properties are generalizable. Therefore, related studies on Ste5 and other substrates, containing different constellations of sites and contributing kinases, will further illuminate the range of regulatory possibilities afforded by multi-site phosphorylation.

In conclusion, our findings indicate that the Ste5 scaffold protein behaves as a regulatory node whereby distinct kinases can target a shared set of phosphorylation sites to jointly control the affinity of a membrane interaction domain. The net impact on the signaling pathway can range from a mild modulation to severe quenching, depending on the regulatory inputs. These properties highlight how multiple phosphorylation sites and collaborating enzymes can expand the options for kinase-mediated regulation. The deep base of knowledge about this pathway offers the opportunity for further insights into how signaling response behaviors can be tuned during evolution, by varying parameters that control recognition and modification by kinases. Finally, the discoveries in this system provide a more general model for how collaborative phosphorylation can facilitate pathway crosstalk by broadening the spectrum of inputs that impinge on a protein target, and they indicate that even well studied kinase pathways might be enhanced by other kinases, including those considered to be antagonistic.

STAR★Methods

Detailed methods are provided in the online version of this paper and include the following:

- KEY RESOURCES TABLES
- CONTACT FOR REAGENT AND RESOURCE SHARING
- METHOD DETAILS
- QUANTIFICATION AND STATISTICAL ANALYSIS

STAR★METHODS

CONTACT FOR REAGENT AND RESOURCE SHARING

Further information and requests for resources and reagents should be directed to and will be fulfilled by the Lead Contact, Alejandro Colman-Lerner (colman-lerner@fbmc.fcen.uba.ar)

EXPERIMENTAL MODEL AND SUBJECT DETAILS

Yeast strains and growth conditions—Standard procedures were used for growth and genetic manipulation of yeast (Sherman, 2002) (Rothstein, 1991). Unless described otherwise, cells were grown at 30°C in yeast extract/peptone (YP) medium or synthetic (SC) medium, containing 2% glucose, galactose, and/or raffinose as carbon sources. Detailed information about yeast strains and plasmids are listed in Tables S3 and S4, respectively.

All *Saccharomyces cerevisiae* strains used in this study are W303 background derivatives (Table S3). Strains for microscopy were derived from TCY3106, a *ste5Δ::natMX4* derivative of ACLY379 (Colman-Lerner et al., 2005), which is a *MAT***a** *bar1Δ* strain. P_{STE5}-*STE5-YFPx3* was introduced at the *TRP1* locus using the *Sna*BI-cut integrating plasmid pPP3379 (and its mutant derivatives). “Loop-in” integration of this plasmid can introduce single or multiple copies, which were distinguished by PCR using primer RS30x-up1 paired with TRP1-dn2 and RS30x-dn2; for strains with multiple insertions, copy number was quantified by total YFP fluorescence.

A two-step (loop-in/loop-out) allele replacement method (Rothstein, 1991) was used to introduce the following mutant alleles at their native genomic loci: *cdc28-as2*, *fus3-as2*, *cdc15-2*, *sst2-T134A*, *gpa1- K21E R22E*, and *ste4-T320A S335A*. Standard PCR-mediated gene deletion and tagging methods (Longtine et al., 1998) were used to introduce *WHI5-mKO$_{kappa}$::HIS3MX6*, *CLN2-myc13::kanMX6*, *CLN2- 3xV5::kanMX6*, *STE5-HTB::natMX6*, *far1Δ::kanMX6*, *cln1Δ::LEU2^{Cg}*, *cln2Δ::kanMX6*, *fus3Δ::kanMX6*, *fus3Δ::hphMX6*, and *kss1Δ::hphMX6*. *P$_{GAL1}$-CLN2*, *P$_{GAL1}$-CLB5*, *P$_{GAL1}$-CLB2*, *P$_{GAL1}$-STE11ΔN-STE7*, and *P$_{MET3}$-CLN2* constructs were integrated at marker loci using plasmids pPP1949, pPP2656, pPP2666, pPP1270, and pCL17, respectively.

Ste5 mutations—Mutations denoted by abbreviated names in the text and figures are specified as follows:

Ste5-ΔPM: Δ48–67 (a.k.a. “ΔNLS” in (Winters et al., 2005))

Ste5-PM*memb: W51N L55N F58N A63N (a.k.a. “NLSb” in (Winters et al., 2005))

Ste5-PM*nuc: E53A K54A R57A F58V Q59A R60A S61A S62A (a.k.a., “NLSm” in (Winters et al., 2005))

Ste5-8A: T4A S11A T29A S43A S69A S71A S81A T102A (Strickfaden et al., 2007)

Ste5-8E: T4E S11E T29E S43E S69E S71E S81E T102E (Strickfaden et al., 2007)

Ste5-16E: T4E P5E S11E P12E T29E P30E S43E P44E S69E P70E S71E P72E S81E P82E T102E P103E (Strickfaden et al., 2007)

Ste5-llpp: L278A L279A P280A P281A (Bhaduri and Pryciak, 2011)

Ste5-ND: Q292A I294A Y295A L307A P310A N315A (Bhattacharyya et al., 2006)

Ste5-4E: T267E S276E T287E S329E (Malleshaiah et al., 2010) (Bhaduri and Pryciak, 2011)

Ste5-4Q: T267Q S276Q T287Q S329Q

Ste5-8SP: T4S T29S T102S

Ste5-n9AN: T6N T41N T87A S91A S104N T118A S120A S126A S132N

METHOD DETAILS

Time-Lapse Microscopy and Ste5 Recruitment Measurements—To assay recruitment of Ste5-YFPx3, membrane and total cell fluorescence was quantified by confocal microscope cytometry as described previously (Bush and Colman-Lerner, 2013). Briefly, exponentially growing cells were placed in 96-well glass-bottom plates (BD Falcon, ~ 10^4 cells/well) pretreated with 1 mg/ml of concanavalin A type V (Sigma-Aldrich). Images were acquired at room temperature (24° C) using an Olympus IX-81 microscope, FV1000 confocal module, and UplanSapo 63x objective (NA 1.35). When YFP and mKO$_{kappa}$ fluorophores were both present, sequential rounds of excitation were performed, and acquisition windows were adjusted to minimize signal crosstalk. For YFP, excitation was at 515 nm and acquisition between 525–540 nm (a wavelength window with particularly

low autofluorescence); for mKO_{kappa}, excitation was at 543 nm and acquisition between 555–580 nm.

Cells were stimulated during imaging with 1 μM α factor (Yale Small Scale Peptide Synthesis, New Haven, CT); for lower concentrations, dilutions were prepared in media containing 40 μg/ml casein (Roche Applied Science) to block unspecific binding to plastics (Colman-Lerner et al., 2005). In each experiment, all cells in an asynchronous population were stimulated simultaneously and for an identical duration. Afterward, the cells in the time-lapse recordings were categorized according to their cell cycle stage at the time of pheromone stimulation. The classification was based on localization of fluorescent Whi5 (tagged with mKO_{kappa}) and/or cell morphology, as follows: cells were classified as G1 if they were initially unbudded, with nuclear Whi5, and remained unbudded 15 minutes after stimulation; cells classified as post-Start were also initially unbudded, but they had cytoplasmic Whi5 (Doncic et al., 2011) and proceeded to form a bud after pheromone stimulation; cells were classified as S-phase if they had a small or incipient bud at the time of stimulation.

Microscopy experiments involving media changes or addition of inhibitors, prior to pheromone stimulation, were performed as follows. Strains with ATP analog-sensitive kinase alleles were pretreated with DMSO or the indicated concentrations of 1-NM-PP1 (Cayman Chemical, Ann Arbor, MI) for 7 min. before adding α factor. Strains with galactose-inducible constructs were pre-incubated overnight in 2% raffinose medium and then switched to 1% raffinose plus 2% galactose for 75 min. prior to addition of pheromone. Strains with a methionine-repressed *CLN2* construct (P_{MET3}-*CLN2*) were switched from methionine-free medium to medium containing 0.2 mg/mL methionine for 60 min. before adding pheromone.

Image segmentation and quantification used Cell-ID (Gordon et al., 2007), and the resulting datasets were analyzed in R (Bush et al., 2012). Membrane recruitment was calculated as the ratio of surface to volume fluorescence, or Srec (Bush and Colman-Lerner, 2013), and expressed as the increase after stimulation (i.e., $Srec[t] - Srec[t_0]$). To analyze cell-to-cell variability, we performed a Principal Component Analysis (PCA), described below. In all charts that plot recruitment as a function of time, the data are shown as the mean (dark line) ± the 95%CI (shaded).

Quantitative analysis of single-cell Ste5 membrane recruitment dynamics—

Our measurement of Ste5 membrane recruitment revealed extensive cell to cell variability (see Fig. 1). This variability is due to a combination of (i) measurement errors, (ii) stochastic fluctuations in the recruitment of Ste5 and (iii) pre-existing differences among cells in one or more cellular states relevant to Ste5 recruitment, such as cell cycle position at the time of stimulation with mating pheromone.

Principal Component Analysis: As the first step towards understanding what factors primarily explained the observed variability, we performed a Principal Component Analysis (PCA). For this analysis, the recruitment statistic (Srec) measured at each time point was treated as a variable, therefore the recruitment dynamics of each cell was represented as a

vector $\bar{v} \in \mathbb{R}^T$, where T is the number of time points (= 10). We applied the analysis to data obtained using the WT strain (MWY003) and retained the first two principal components (PC_1 and PC_2), since together they explained 78% of the variance within the population. Notably, we found a clear correlate of PC_1 and PC_2 in two characteristics of the recruitment dynamics: PC_1 roughly captures the mean recruitment level, while PC_2 reflects the observed amount of detachment from the membrane (decline) (see Figure 1G).

Fitting vectors derived from PCA to recruitment data: The analysis above indicates that cells predominantly differed from each other in their average recruitment level and in the degree to which the initially recruited Ste5 later detached from the membrane. Thus, to analyze the effects of experimental treatments and mutations, we condensed the single cell data to represent each cell by two calculated values: the initial recruitment and the degree of detachment. To minimize contributions from noise and stochastic fluctuations in the raw data, we calculated these values from fitted curves, as described below.

We defined two orthonormal vectors based on PCA results of the WT strain: the mean recruitment vector $\bar{r} = \frac{1}{\sqrt{8}}[0,0,1,1,1,1,1,1,1,1,]$ and the decline vector $\bar{d}$ = [0,0,0.689,0.373,0.138,−0.0374,−0.168,−0.265,−0.337,−0.392]. We fitted the decline vector $\bar{d}$ as an exponential decline to PC_2, restricted to the orthonormality condition ($\bar{r} \cdot \bar{d} = 0$ and $\|\bar{d}\| = 1$). We therefore defined the recruitment and decline scores of each cell as $S_r = \bar{r} \cdot \bar{v}$ and $S_d = \bar{d} \cdot \bar{v}$, respectively. Then, we calculated the projected dynamics of each cell on the subspace defined by $\bar{r}$ and $\bar{d}$ by $\bar{p} = S_r\bar{r} + S_d\bar{d}$. (Examples comparing the projected and raw dynamics are shown in Figure 1G.) Finally, we defined the two biologically relevant variables, calculated from the projected dynamics: the initial recruitment (iRec), which corresponds to the 3-rd component of $\bar{p}$, and the degree of decline (% Decline), defined as $D_f = 100\left(\frac{R_{\max} - R_{\min}}{R_i}\right)\mathrm{sgn}(S_d)$, where $R_{\max} = \max_{2<i\leq T}\{p_i\}$, $R_{\min} = \min_{2<i\leq T}\{p_i\}$, and *sgn* is the sign function.

Note that because iRec and D_f were calculated from the projected data $\bar{p}$, they are less susceptible to measurement noise as well as to stochastic fluctuations in Ste5 recruitment than if they had been calculated from the raw data $\bar{p}$. Thus, the reported values for initial recruitment and % decline, which appear in bar graphs and histograms in Figures throughout the paper, were calculated using the fitted variables. The calculation of % decline was performed only for cells with initial recruitment above the threshold of 0.06.

In Vivo Phosphorylation Assays—Plasmids expressing HA-tagged Ste5 fragments were transformed into *cdc15-2* strains (MWY198, except where indicated otherwise). To obtain synchronous cultures, the *cdc15-2* cultures were grown at 25°C, arrested at 37°C for 3 hr, then released by transfer to 25°C (using shaking water baths). Aliquots were collected at times of low and high Cln2 levels (20 and 80 min., corresponding to G1 and S, respectively). Before harvesting, cells were incubated ± α factor (1 μM) for 5 min. (For experiments using kinase inhibitors, cells were collected at 15 and 75 min. and pre-treated with 10 μM 1NM-PP1 for 5 min. before α factor.) Then, 2 mL of culture was collected by centrifugation, and cell pellets were frozen before preparation of whole cell extracts.

Other Signaling Assays—Transcriptional response to pheromone treatment was measured using a *FUS1-lacZ* reporter plasmid (pSB231) and β-galactosidase activity assay Specifically, after recording the OD_{660}, cells from 1 mL of culture were harvested by centrifugation, resuspended in 0.5 mL of Z buffer (82 mM sodium phosphate [pH 7.0], 10 mM KCl, 1 mM $MgSO_4$, 40 mM β-mercaptoethanol), and permeabilized by vortexing in the presence of 0.01 mL of 0.4% sodium dodecyl sulfate and 0.05 mL of chloroform. Reactions were started by adding 0.3 mL of *o*-nitrophenyl-β-D-galactopyranoside (2.4 mg/mL in Z buffer), incubated at 30° for 5 to 300 min., stopped by adding 0.5 mL of 1 M Na_2CO_3, and stored on ice until all reactions were finished. Reaction mixtures were clarified in a microcentrifuge (full speed, 5 min.), and then 1 mL supernatant was collected to measure the OD_{420}. β-Galactosidase activity was calculated as $(1000 \times OD_{420}) \div (OD660 \times$ culture volume [mL] × reaction time [min.]).. Activation of the MAPK Fus3 was assayed by immunoblotting of whole cell extracts (described in the next section) and, where indicated, quantified by densitometry using ImageJ.

To measure effects of P_{GAL1}-*CLN2* on pheromone response, cells were grown in 2% raffinose selective media, induced with 2% galactose for 75 min., and then treated with 0.1 μM α factor. To measure transcriptional response, α factor treatment proceeded for 90 min.. To measure MAPK phosphorylation, α factor treatment was for 0–15 min., as indicated.

To measure Fus3 activation kinetics in P_{GAL1}-*CLN2 cdc28-as2* strains, after inducing with galactose induction for 75 min., cells were incubated with varying concentrations of 1NM-PP1 for 5 min. before adding α factor (0.1 μM), and 2-mL samples were collected at various times before and afterwards. The first sample (0 min.) was collected immediately before α factor treatment. After α factor treatment, samples were collected and transferred to 2-mL microcentrifuge tubes 90 sec. before the designated stop time (2, 5, or 15 min.), to allow sufficient time to collect and freeze cell pellets; i.e., cells were harvested by centrifugation for 30 sec., supernatants were aspirated, and cell pellets were frozen by placing the tubes in a liquid nitrogen bath at the designated stop time.

For experiments measuring Fus3 activation in synchronous cultures, cells in SC + glucose medium were first arrested in G1 using α factor (50 nM, 2 hr). Then, cells were pelleted, washed twice with fresh medium, suspended in fresh medium, and incubated at 30°C. Control experiments indicate that, after release, phospho-Fus3 returns to basal levels by 10–15 min., and Cln2 levels peak by 45 min. Thus, to compare Fus3 activation by different Ste5 mutants in G1 and S phase, aliquots were collected at 15 min (G1) or 45 min (S), and briefly re-stimulated with α factor (50 nM, 15 min.). To measure the kinetics of Fus3 activation at different cell cycle stages, cell aliquots were collected at 10-min intervals (from 15 to 105 min.) after release from α factor arrest, and then re-stimulated with 50 nM α factor for various times (0, 2, 5, and 15 min.) using the procedure described above. For related experiments in *cdc28-as2* and *fus3-as2* strains, cell aliquots were collected at different times after release (15, 45, or 75 min.), treated with the indicated concentrations of 1NM-PP1 for 5 min., then re-stimulated with 50 nM α factor for 0–15 min., as above.

Whole Cell Extracts and Immunoblotting—Whole cell extracts were prepared using frozen cell pellets from 2 mL cultures (OD660 ~ 0.6), by lysis in trichloroacetic acid (TCA).

Specifically, 300 μL of TCA buffer (10 mM Tris-HCl, pH 8.0, 10% TCA, 25 mM ammonium acetate, 1 mM Na_2EDTA) was added directly to frozen cell pellets, and incubated on ice for 10 minutes. Samples were pelleted in a microcentrifuge for 10 min at 4°C. The pellet was resuspended in 75 μL Resuspension Buffer (0.1 M Tris.HCl, pH 11.0, 3% SDS), boiled for 5 min, allowed to cool at room temperature for 5 minutes, then re-centrifuged for 30 sec. The supernatant (60 μL) was transferred to a new tube, 10 μL was reserved to assay protein concentration, and then 50 μL of 2x SDS Sample Buffer was added to the remainder. Total protein concentrations were measured by BCA assay (Pierce #23225), and equal amounts (usually 20 μg) were loaded per lane.

Proteins were resolved by SDS-PAGE and transferred to PVDF in a submerged tank. Primary antibodies were mouse anti-HA (1:1000, Covance #MMS101R) and anti-V5 (1:5000, Invitrogen #46-0705), rabbit anti-myc (1:200 Santa Cruz Biotechnologies #sc-789), anti-phospho-p44/42 (1:1000, Cell Signaling Technology #9101 or #4370), and anti-G6PDH (1:100000, Sigma #A9521), and goat anti-Fus3 (1:2000, Santa Cruz Biotechnologies #sc-6773). HRP-conjugated secondary antibodies were goat antimouse (1:3000, BioRad #170-6516), goat anti-rabbit (1:3000, Jackson ImmunoResearch #111-035-144), or donkey anti-goat (1:3000 Santa Cruz #sc-2020). Enhanced chemilluminescent detection used a BioRad Clarity kit (#170-5060).

Mass Spectrometry Analysis of Ste5 Phosphorylation

Sample Preparation: Using the *cdc15-2* strain PPY2466, a Ste5-HTB fusion protein was purified from synchronized cultures to assess the effect of pheromone (G1 cells ± α factor) and cell cycle entry (G1 vs. S-phase cells). Three independent experimental replicates were performed. For each replicate, we inoculated three YPD cultures (1 L for replicate #1, or 500 mL for replicates #2–3), which were incubated (with shaking) overnight at 25°C until $OD_{600} = 1$. Then, each culture was diluted with an equal volume of pre-warmed (37°C) YPD, and incubated at 37°C for 2.5 hours; M- phase arrest was confirmed by microscopy. Next, cells in each culture were collected by filtration, suspended in 1 L of 25°C YPD, and incubated at 25°C. Aliquots were removed at several time points to monitor cell cycle progression by microscopy (budding index). The three cultures were treated and harvested as follows: (a) the first culture was released from M-phase arrest for 5 min., treated with 1.2 μM α factor for 5 min., then harvested; (b) the second culture was released for 5 min., treated with methanol (mock) for 5 min., then harvested; (c) the third culture was released for 70 min., then harvested (without α factor treatment). Note that we did not perform pheromone treatment of the 70-min. cultures; this is because the arrested cultures did not release with optimal synchrony, and so a significant fraction of G1 cells potentially remained after 70 min. (Specifically, in the three experimental replicates, only 60, 66, and 69% of cells formed a small bud by 70 min.). Hence, any pheromone-induced changes in these cultures would be ambiguous as to whether they had occurred in the S-phase cells versus the minor fraction whose delayed release left them in late M or G1 phase.

Cells were harvested by filtration and frozen in liquid nitrogen. Using methods optimized previously (Reiter et al., 2012), tandem affinity purification was performed from denatured lysates as follows. Cells were pulverized in a cryogenic grinder (SPEX Freezer Mill 6770 or

6870, SPEXSamplePrep, Metuchen, NJ), using seven rounds (3 min breakage at 15 cycles per second, then 3 min cooling). The cell powder was suspended in denaturing buffer (6 M guanidine HCl, 50 mM Tris-HCl, 5 mM NaF, 1 mM PMSF, 0.1% Tween, protease inhibitor cocktail [Roche, Basel, Switzerland, #11-873-580-001], pH 8) and cleared of debris by centrifugation (10,000 × *g*, 15 min, 4°C). Extracts were incubated for 4 hr wi th Ni^{2+}-Sepharose beads (GE Healthcare, Buckinghamshire, UK, #17-5318-06). The beads were washed twice with urea buffer (8M urea, 50 mM Na-PO_4, 300 mM NaCl, 0.01% Tween, pH 8), then thrice with urea buffer pH 6.3. Proteins were eluted in three consecutive steps using urea buffer pH 4.3 with 10 mM EDTA. Eluates were combined, incubated overnight with streptavidin-agarose beads, then washed three times with urea wash buffer containing 1% SDS and three times with pure urea wash buffer. Proteins were digested overnight with trypsin (Trypsin Gold, Promega). The overnight digest was stopped with 1% trifluoroacetic acid and the peptides were desalted using C18 Stagetips (Thermo Scientific Pierce, #87782).

Mass Spectrometry Methods: Peptides from overnight trypsin digestion were separated on an Ultimate 3000 RSLC nano-flow chromatography system (Thermo-Fisher), using a pre-column for sample loading (Acclaim PepMap C18, 2 cm × 0.1 mm, 5 μm, Thermo-Fisher), and a C18 analytical column (Acclaim PepMap C18, 50 cm × 0.75 mm, 2 μm, Thermo-Fisher), applying a segmented linear gradient from 2% to 80% solvent B (solvent B: 80% acetonitrile, 0.1% formic acid; solvent A: 0.1% formic acid) at a flow rate of 230 nL/min over 120 min. Peptides were subsequently analyzed on a Q Exactive Plus Orbitrap mass spectrometer (Thermo Fisher), which was coupled to the column with a Proxeon nanospray flex ion source (Thermo Fisher) using coated emitter tips (New Objective). The capillary temperature was set to 275°C.

The mass spectrometer was operated in data-dependent mode, survey scans were obtained in a mass range of 380–1650 m/z with lock mass activated, at a resolution of 70,000 at 200 m/z and an automatic gain control (AGC) target value of 3E6. The 12 most intense ions were selected for fragmentation in the higher-energy collision dissociation (HCD) cell at 27% collision energy. Multi-stage mass spectrometry (MSn) scans were obtained at a resolution of 17,500 at 200 m/z, an AGC target value of 1E5, 500 milliseconds maximum ion injection time and 2 m/z isolation window. The intensity threshold for precursor selection was set to 4E4, peptides with a charge of +1 were excluded from fragmentation, the peptide match feature was set to on, the exclude isotope feature was enabled and selected precursors were dynamically excluded from repeated sampling for 30 seconds. A total of 26 HPLCMS/MS runs were recorded. MS proteomics data have been deposited to the ProteomeXchange Consortium through the Proteomics Identifications database (PRIDE) (Vizcaino et al., 2016) partner repository with the data set identifiers PDX006154.

Label-free quantification (LFQ) of the mass spectrometry measurements was achieved by comparing the intensities of MS1 peak areas of peptides between multiple LC-MS runs. Ratios were calculated for pairwise comparisons of the three treatment conditions: (i) 10 min. + pheromone vs. 10 min. (mock), (ii) 70 min vs. 10 min. (mock), and 10 min. + pheromone vs. 70 min. These ratios were expressed as log2 values. Raw MS data was analyzed using in-house developed scripts utilizing the Python library Maspy (Hollenstein and Hollenstein, 2017) and several additional external programs, as described below.

Computational methods for MS-data analysis: A total of 26 HPLC-MS/MS runs were recorded from three biological replicates per experimental condition. All files were deposited to the ProteomeXchange Consortium through the Proteomics Identifications database (PRIDE) (Vizcaino et al., 2016) partner repository with the data set identifier PDX006154. Raw data was analyzed using in-house developed scripts utilizing the Python library Maspy (Hollenstein and Hollenstein, 2017) (release 1.1.3) and several additional external programs.

Acquired Q Exactive Plus RAW files were converted to mzML files, using msConvert from the open source software Proteowizard (Chambers et al., 2012) (version 3.0.9992). Peak picking was performed on MS1 and MS2 level with the option “Prefer Vendor” activated, zlib compression was used and the binary encoding precision was set to 32 bit. The monoisotopic m/z value and charge state of MS2 precursors were recalculated and exported from RAW to MGF files using "Spectrum Selector" and "Spectrum Exporter" nodes of the software Proteome Discoverer (version 2.1, Thermo Fisher). For peptide spectrum matching, we used the open source program Comet (Eng et al., 2013) (version 2015011), in combination with Percolator (Kall et al., 2007) (version 2.08) for estimation of the false discovery rate (FDR) and the Java standalone version of phosphoRS (Taus et al., 2011) for calculation of phosphorylation site localization probabilities. MS2 spectra were searched against a protein database from the SGD (Saccharomyces Genome Database, www.yeastgenome.org, version 3rd February 2011) containing 6,717 entries, concatenated with a database of 248 common laboratory contaminants (provided with MaxQuant (Tyanova et al., 2015)). A reverse database was generated by inverting protein amino acid sequences. Comet searches were performed separately against the forward and reverse databases. The following Comet search parameters were used for the initial search; carbamidomethylation of cysteine residues were set as fixed, oxidation of methionine and n-terminal acetylation as variable modifications. Up to two variable modifications per peptide were allowed. The precursor mass tolerance was set to 10 ppm, fragment bin tolerance was set to 0.03 with an offset of 0. Enzyme specificity was set to full trypsin, with allowed cleavage after proline and up to two missed cleavage events. Variable removal of protein n-terminal methionine was allowed. For the main search, the number of allowed variable modifications per peptide was increased to three, and additional variable modifications were added; phosphorylation of serine, threonine, tyrosine and deamidation of asparagine and glutamine. Percolator and phosphoRS were used with standard settings. Peptide spectrum matches were filtered to a q-value of 0.01, corresponding to an FDR of 1%. Phosphorylation sites with an isoform probability of greater than or equal to 70% were considered as confidently localized. The open source program Dinosaur (Teleman et al., 2016) (1.1.3) was used to define peptide LC-MS features on the MS1 level, standard settings were used.

The above settings were used in the following workflow. Mono isotopic mass and charge state of MS2 precursor ions were replaced with values extracted from the MGF file generated by Proteome Discoverer. Exact mass of identified peptides from the initial Comet database search were used to calibrate the m/z value of MS1 ions and MS2 precursors. First the m/z dependent error was corrected using a fitted spline function, then the retention time dependent error was corrected separately for each scan by the median of the remaining

relative m/z deviation. New mzML files were generated containing the corrected values. These files were used to perform the Comet main search and to run Dinosaur. LC-MS features were annotated with peptide spectrum matches using the following settings. Maximum relative deviation was set to 2 ppm between exact calculated mass value of peptides and observed LC-MS feature masses, equal charge state and MS2 retention time within the retention time boundaries of the LC-MS feature. Ambiguous peptide assignment was resolved by only considering the one with the best Percolator e-value. For retention time alignment processing groups were defined by grouping LC-MS runs that were measured in a batch on the same HPLC-MS system. Here, we defined three processing groups, see Table M4 associated with PRIDE dataset PDX006154. Retention time alignment was performed using Maspy. LC-MS runs within each group were aligned to a reference run (see Table M4, cited above). For calculation of retention time deviation only annotated features were considered. No minimal feature intensity was used. m/z deviation was set to 2 ppm. Retention time deviation was set to 60 seconds for group 1 and 80 seconds for group 2 and 3. LC-MS features of LC-MS runs within the same processing group were clustered to generate label-free quantification feature groups (LFQ-FG) using a quality threshold approach implemented in Maspy. Threshold levels were set to a time limit of 40 seconds and a mass limit of 5 ppm. LFQ-FGs were annotated via the PSM with the best Percolator e-value. For phosphorylation site assignment only PSMs with the annotated peptide sequence and a phosphorylation isoform probability above 70% were considered. PSM phosphorylation isoform probability of individual isoforms were added up. The isoform with the highest total sum was used for phosphorylation site assignment of the LFQ-FG.

We observed an increased intensity fluctuation between LC-MS runs that were injected twice from the same autosampler vial. To account for these effects, processing groups were subdivided into quantification groups, which contained runs from either the first or the second injection. Intensity normalization and relative quantification steps were performed separately within these quantification groups. As described by Lyutvinskiy et. al (Lyutvinskiy et al., 2013) LC-MS measurements are often affected by a time dependent drift in LC-MS feature abundance. Time dependent normalization of LC-MS feature intensities was performed by using a spline function. Peptides containing methionine or tryptophan and peptides from Ste5 were excluded for calculation of the spline functions. Normalization was performed separately within each quantification group and intensity deviations were calculated relative to a reference run (see Table M4, cited above). In addition, we observed a varying degree of methionine and tryptophan oxidation between LC-MS runs. These differences were normalized separately within each quantification group and relative to a reference run. Correction factors were calculated independently for peptides containing an oxidized amino acid or not, excluding peptides from Ste5. Peptides lacking oxidized amino acids were corrected dependent on the total number of methionine and tryptophan amino acids. Oxidized peptides were corrected in dependence of the number of oxidized amino acids.

Label-free quantification (Table S2) was performed as follows. Peptides were sorted into so called phosphoislands (Langella et al., 2017) that contain adjacent phosphorylation sites covered by overlapping peptides. Phosphoislands were generated by grouping phosphopeptides that overlap by at least one of the phosphorylated amino acids. The amino

acid sequence and number of phosphosites may vary between the overlapping peptides. For each phosphoisland one or multiple phosphorylation site groups (PSG) (Romanov et al., 2017) and one unphosphorylated counter group (UCG) were defined. Phosphopeptides containing the same set of phosphorylated residues constitute a unique PSG. However, oxidized and not oxidized phosphopeptides were treated separately. A UCG contained all unphosphorylated peptides that overlap with at least one of the phosphoislands phosphorylation sites. In addition, a tag group (TG) was defined and used for calculation of a protein abundance normalization factor. The TG contained all peptides that did not overlap with the native Ste5 protein sequence and were neither phosphorylated nor oxidized. For LFQ only LFQ-FGs annotated with a peptide of Ste5 that were either not phosphorylated or had an isoform probability higher than the cutoff of 70% were considered. LFQ experiments were compared pairwise and independently for each replicate pair. LFQ-FG intensities were only compared within quantification groups. The LFQ-FG log2 intensities from multiple technical replicates of the same quantification group were averaged, only LFQ-FGs with an intensity value in both replicates of the respective condition were considered for quantification. A protein abundance normalization factor was calculated by averaging the log2 intensities of the TG and calculating the difference of the averaged log2 intensities. For PSG and UCG the log2 intensities of each replicate were corrected by the protein abundance factor and averaged. Log2 ratios were calculated as the difference of the averaged log2 intensities. For label-free quantification on the peptide level (Table M3 - associated with PRIDE dataset PDX006154), LFQ-FGs were clustered according to chemical modifications of peptides. Peptides having the same amino acid sequence, the same number and positions of phosphorylation sites and protein n-terminal acetylation sites, and the same number and type of other chemical modifications (oxidation and deamidation - however, independent of their position) were grouped. All other steps (such as filtering, quantification and normalization) were carried out as described above for PSG and UCG.

QUANTIFICATION AND STATISTICAL ANALYSIS

All Ste5 recruitment measurements correspond to at least three replicate experiments, and the results shown correspond to data pooled from all replicates. Distributions of initial recruitment of Ste5 and percent decline were compared using the two-sample Kolmogorov-Smirnoff test, and bar graphs with a Fisher exact test . The results of all comparisons tested appear in Table S1.

DATA AND SOFTWARE AVAILABILITY

Data Resources—Original microscopy images and time-lapse movies are available at Mendeley Data http://dx.doi.org/10.17632/w75s7vkjfy.3. Original images of western blot data are available at Mendeley Data: http://dx.doi.org/10.17632/6k88nmjvdm.1. Mass spectrometry data are available at the PRIDE Archive: https://www.ebi.ac.uk/pride/archive/projects/PXD006154.

Supplementary Material

Refer to Web version on PubMed Central for supplementary material.

Acknowledgments

We thank D. McCollum, N. Rhind, G. Vasen, G. Pesce, A. Srebrow, and A. Constantinou for their comments on the manuscript. This work was supported by grants from the National Institutes of Health (GM057769 to PMP and GM097479 to ACL), from the Argentine Agency of Research and Technology (PICT2010-2248 and PICT2013-2210) to ACL, and from the Austrian Science Fund (project F34) and Verein zur Förderung der Genomforschung to GA.

References

Alon, U. An Introduction to Systems Biology: Design Principles of Biological Circuits. Chapman & Hall/CRC Mathematical & Computational Biology; Chapman & Hall; 2006.

Alvaro CG, Thorner J. Heterotrimeric G Protein-coupled Receptor Signaling in Yeast Mating Pheromone Response. J Biol Chem. 2016; 291:7788–7795. [PubMed: 26907689]

Bardwell L. A walk-through of the yeast mating pheromone response pathway. Peptides. 2005; 26:339–350. [PubMed: 15690603]

Bhaduri S, Pryciak PM. Cyclin-specific docking motifs promote phosphorylation of yeast signaling proteins by G1/S Cdk complexes. Curr Biol. 2011; 21:1615–1623. [PubMed: 21945277]

Bhattacharyya RP, Remenyi A, Good MC, Bashor CJ, Falick AM, Lim WA. The Ste5 scaffold allosterically modulates signaling output of the yeast mating pathway. Science. 2006; 311:822–826. [PubMed: 16424299]

Bishop AC, Ubersax JA, Petsch DT, Matheos DP, Gray NS, Blethrow J, Shimizu E, Tsien JZ, Schultz PG, Rose MD, et al. A chemical switch for inhibitor-sensitive alleles of any protein kinase. Nature. 2000; 407:395–401. [PubMed: 11014197]

Bush A, Chernomoretz A, Yu R, Gordon A, Colman-Lerner A. Using Cell-ID 1.4 with R for microscope-based cytometry. Curr Protoc Mol Biol. 2012 Chapter 14, Unit 14 18.

Bush A, Colman-Lerner A. Quantitative measurement of protein relocalization in live cells. Biophys J. 2013; 104:727–736. [PubMed: 23442923]

Chambers MC, Maclean B, Burke R, Amodei D, Ruderman DL, Neumann S, Gatto L, Fischer B, Pratt B, Egertson J, et al. A cross-platform toolkit for mass spectrometry and proteomics. Nat Biotechnol. 2012; 30:918–920. [PubMed: 23051804]

Colman-Lerner A, Gordon A, Serra E, Chin T, Resnekov O, Endy D, Pesce CG, Brent R. Regulated cell-to-cell variation in a cell-fate decision system. Nature. 2005; 437:699–706. [PubMed: 16170311]

Conlon P, Gelin-Licht R, Ganesan A, Zhang J, Levchenko A. Single-cell dynamics and variability of MAPK activity in a yeast differentiation pathway. Proc Natl Acad Sci U S A. 2016; 113:E5896–E5905. [PubMed: 27651485]

Doncic A, Atay O, Valk E, Grande A, Bush A, Vasen G, Colman-Lerner A, Loog M, Skotheim JM. Compartmentalization of a bistable switch enables memory to cross a feedback-driven transition. Cell. 2015; 160:1182–1195. [PubMed: 25768911]

Doncic A, Falleur-Fettig M, Skotheim JM. Distinct interactions select and maintain a specific cell fate. Mol Cell. 2011; 43:528–539. [PubMed: 21855793]

Durandau E, Aymoz D, Pelet S. Dynamic single cell measurements of kinase activity by synthetic kinase activity relocation sensors. BMC Biol. 2015; 13:55. [PubMed: 26231587]

Eng JK, Jahan TA, Hoopmann MR. Comet: an open-source MS/MS sequence database search tool. Proteomics. 2013; 13:22–24. [PubMed: 23148064]

Feng Y, Song LY, Kincaid E, Mahanty SK, Elion EA. Functional binding between Gbeta and the LIM domain of Ste5 is required to activate the MEKK Ste11. Curr.Biol. 1998; 8:267–278. [PubMed: 9501067]

Godfrey M, Touati SA, Kataria M, Jones A, Snijders AP, Uhlmann F. PP2A(Cdc55) Phosphatase Imposes Ordered Cell-Cycle Phosphorylation by Opposing Threonine Phosphorylation. Mol Cell. 2017; 65:393–402. e393. [PubMed: 28132839]

Gordon A, Colman-Lerner A, Chin TE, Benjamin KR, Yu RC, Brent R. Single-cell quantification of molecules and rates using open-source microscope-based cytometry. Nat Methods. 2007; 4:175–181. [PubMed: 17237792]

Hartwell LH, Culotti J, Pringle JR, Reid BJ. Genetic control of the cell division cycle in yeast. Science. 1974; 183:46–51. [PubMed: 4587263]

Hollenstein, DM., Hollenstein, JJ. hollenstein/maspy 1.1.3. 2017. (http://doi.org/10.5281/zenodo.345118)

Inouye C, Dhillon N, Thorner J. Ste5 RING-H2 domain: role in Ste4-promoted oligomerization for yeast pheromone signaling. Science. 1997; 278:103–106. [PubMed: 9311911]

Kall L, Canterbury JD, Weston J, Noble WS, MacCoss MJ. Semi-supervised learning for peptide identification from shotgun proteomics datasets. Nat Methods. 2007; 4:923–925. [PubMed: 17952086]

Koivomagi M, Ord M, Iofik A, Valk E, Venta R, Faustova I, Kivi R, Balog ER, Rubin SM, Loog M. Multisite phosphorylation networks as signal processors for Cdk1. Nat Struct Mol Biol. 2013; 20:1415–1424. [PubMed: 24186061]

Koivomagi M, Valk E, Venta R, Iofik A, Lepiku M, Balog ER, Rubin SM, Morgan DO, Loog M. Cascades of multisite phosphorylation control Sic1 destruction at the onset of S phase. Nature. 2011; 480:128–131. [PubMed: 21993622]

Langella O, Valot B, Balliau T, Blein-Nicolas M, Bonhomme L, Zivy M. X!TandemPipeline: A Tool to Manage Sequence Redundancy for Protein Inference and Phosphosite Identification. J Proteome Res. 2017; 16:494–503. [PubMed: 27990826]

Longtine MS, McKenzie A III, Demarini DJ, Shah NG, Wach A, Brachat A, Philippsen P, Pringle JR. Additional modules for versatile and economical PCR-based gene deletion and modification in Saccharomyces cerevisiae. Yeast. 1998; 14:953–961. [PubMed: 9717241]

Lyutvinskiy Y, Yang H, Rutishauser D, Zubarev RA. In silico instrumental response correction improves precision of label-free proteomics and accuracy of proteomics based predictive models. Mol Cell Proteomics. 2013; 12:2324–2331. [PubMed: 23589346]

Maeder CI, Hink MA, Kinkhabwala A, Mayr R, Bastiaens PI, Knop M. Spatial regulation of Fus3 MAP kinase activity through a reaction-diffusion mechanism in yeast pheromone signalling. Nat Cell Biol. 2007; 9:1319–1326. [PubMed: 17952059]

Malleshaiah MK, Shahrezaei V, Swain PS, Michnick SW. The scaffold protein Ste5 directly controls a switch-like mating decision in yeast. Nature. 2010; 465:101–105. [PubMed: 20400943]

McGrath DA, Balog ER, Koivomagi M, Lucena R, Mai MV, Hirschi A, Kellogg DR, Loog M, Rubin SM. Cks confers specificity to phosphorylation-dependent CDK signaling pathways. Nat Struct Mol Biol. 2013; 20:1407–1414. [PubMed: 24186063]

Oehlen LJ, Cross FR. G1 cyclins CLN1 and CLN2 repress the mating factor response pathway at Start in the yeast cell cycle. Genes Dev. 1994; 8:1058–1070. [PubMed: 7926787]

Pinna LA, Ruzzene M. How do protein kinases recognize their substrates? Biochimica et Biophysica Acta (BBA) - Molecular Cell Research. 1996; 1314:191–225. [PubMed: 8982275]

Reiter W, Anrather D, Dohnal I, Pichler P, Veis J, Grotli M, Posas F, Ammerer G. Validation of regulated protein phosphorylation events in yeast by quantitative mass spectrometry analysis of purified proteins. Proteomics. 2012; 12:3030–3043. [PubMed: 22890988]

Romanov N, Hollenstein DM, Janschitz M, Ammerer G, Anrather D, Reiter W. Identifying protein kinase-specific effectors of the osmostress response in yeast. Sci Signal. 2017; 10

Rothstein, R. Targetting, disruption, replacement, and allele rescue: integrative DNA transformation in yeast. In: Guthrie, C., Fink, GR., editors. Methods in Enzymology. San Diego, California 92101: Academic Press; 1991. p. 281-301.

Sherman F. Getting started with yeast. Methods Enzymol. 2002; 350:3–41. [PubMed: 12073320]

Strickfaden SC, Pryciak PM. Distinct roles for two Galpha-Gbeta interfaces in cell polarity control by a yeast heterotrimeric G protein. Mol Biol Cell. 2008; 19:181–197. [PubMed: 17978098]

Strickfaden SC, Winters MJ, Ben-Ari G, Lamson RE, Tyers M, Pryciak PM. A mechanism for cell-cycle regulation of MAP kinase signaling in a yeast differentiation pathway. Cell. 2007; 128:519–531. [PubMed: 17289571]

Suzuki K, Sako K, Akiyama K, Isoda M, Senoo C, Nakajo N, Sagata N. Identification of non-Ser/Thr-Pro consensus motifs for Cdk1 and their roles in mitotic regulation of C2H2 zinc finger proteins and Ect2. Scientific reports. 2015; 5:7929. [PubMed: 25604483]

Taus T, Kocher T, Pichler P, Paschke C, Schmidt A, Henrich C, Mechtler K. Universal and confident phosphorylation site localization using phosphoRS. J Proteome Res. 2011; 10:5354–5362. [PubMed: 22073976]

Teleman J, Chawade A, Sandin M, Levander F, Malmstrom J. Dinosaur: A Refined Open-Source Peptide MS Feature Detector. J Proteome Res. 2016; 15:2143–2151. [PubMed: 27224449]

Tyanova S, Temu T, Carlson A, Sinitcyn P, Mann M, Cox J. Visualization of LC-MS/MS proteomics data in MaxQuant. Proteomics. 2015; 15:1453–1456. [PubMed: 25644178]

Vizcaino JA, Csordas A, del-Toro N, Dianes JA, Griss J, Lavidas I, Mayer G, Perez-Riverol Y, Reisinger F, Ternent T, et al. 2016 update of the PRIDE database and its related tools. Nucleic Acids Res. 2016; 44:D447–456. [PubMed: 26527722]

Winters MJ, Lamson RE, Nakanishi H, Neiman AM, Pryciak PM. A membrane binding domain in the ste5 scaffold synergizes with gbetagamma binding to control localization and signaling in pheromone response. Mol Cell. 2005; 20:21–32. [PubMed: 16209942]

Yang X, Lau KY, Sevim V, Tang C. Design principles of the yeast G1/S switch. PLoS Biol. 2013; 11:e1001673. [PubMed: 24130459]

Yu RC, Pesce CG, Colman-Lerner A, Lok L, Pincus D, Serra E, Holl M, Benjamin K, Gordon A, Brent R. Negative feedback that improves information transmission in yeast signalling. Nature. 2008; 456:755–761. [PubMed: 19079053]

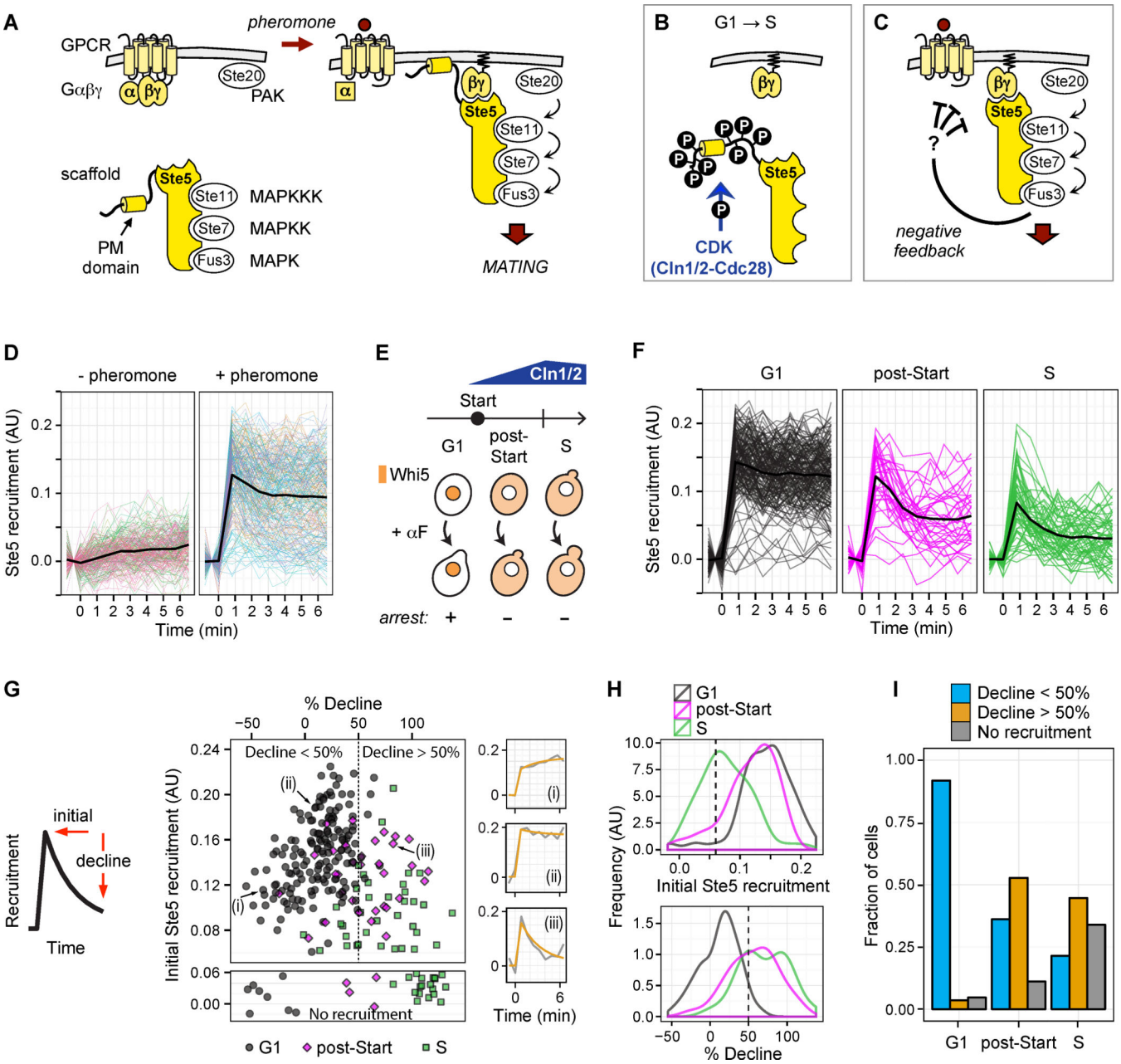

Figure 1. Single-cell assays reveal cell cycle stage-specific recruitment dynamics

(A) Pheromone stimulates plasma membrane recruitment of Ste5, which binds Gβγ (via its RING-H2 domain) and membrane phospholipids (via its PM domain).

(B) At the G1 to S transition, CDK inhibits Ste5 by phosphorylating sites near the PM domain

(C) Negative feedback from the MAPK Fus3 dampens Ste5 recruitment via an unknown target.

(D) Membrane recruitment dynamics. Black lines show mean results. Thin colored lines show individual cell traces, to illustrate variability. In these and all related plots, Ste5-YFPx3 membrane recruitment was calculated as the ratio of surface to volume fluorescence, and

expressed as the increase after pheromone stimulation. See Method Details. AU, arbitrary units.

(E) Cell cycle stage classification was based on localization of fluorescent Whi5 (orange) and/or on morphology before and after stimulation with α factor (αF). G1 cells are unbudded, have nuclear Whi5, and remain unbudded 15 minutes after stimulation (at which time a mating projection may form, as shown); post-Start cells are also initially unbudded, but have cytoplasmic Whi5 (Doncic et al., 2011) and produce a bud despite stimulation; S-phase cells have a small or incipient bud at the time of stimulation.

(F) Ste5 recruitment dynamics at distinct stages of the G1 to S phase transition. Note the "peak and decline" behavior in post-Start and S-phase cells.

(G) Cell-to-cell variation is explained by two variables: initial recruitment and extent of decline. The dashed line defines two categories: declines < 50% or > 50%. A third category contains cells with no recruitment (i.e., below 0.06 initial recruitment, within that shown by 98% of untreated cells). *Right*, three examples (i-iii) of single cell dynamics (grey, raw data; orange, exponential fit — see Method Details).

(H) Histograms show the distribution of cells along each measurement axis from panel G. Dashed lines mark the category thresholds used throughout this study.

(I) Distribution of cells among three recruitment categories, at each cell cycle stage. Strain: VRY5013.

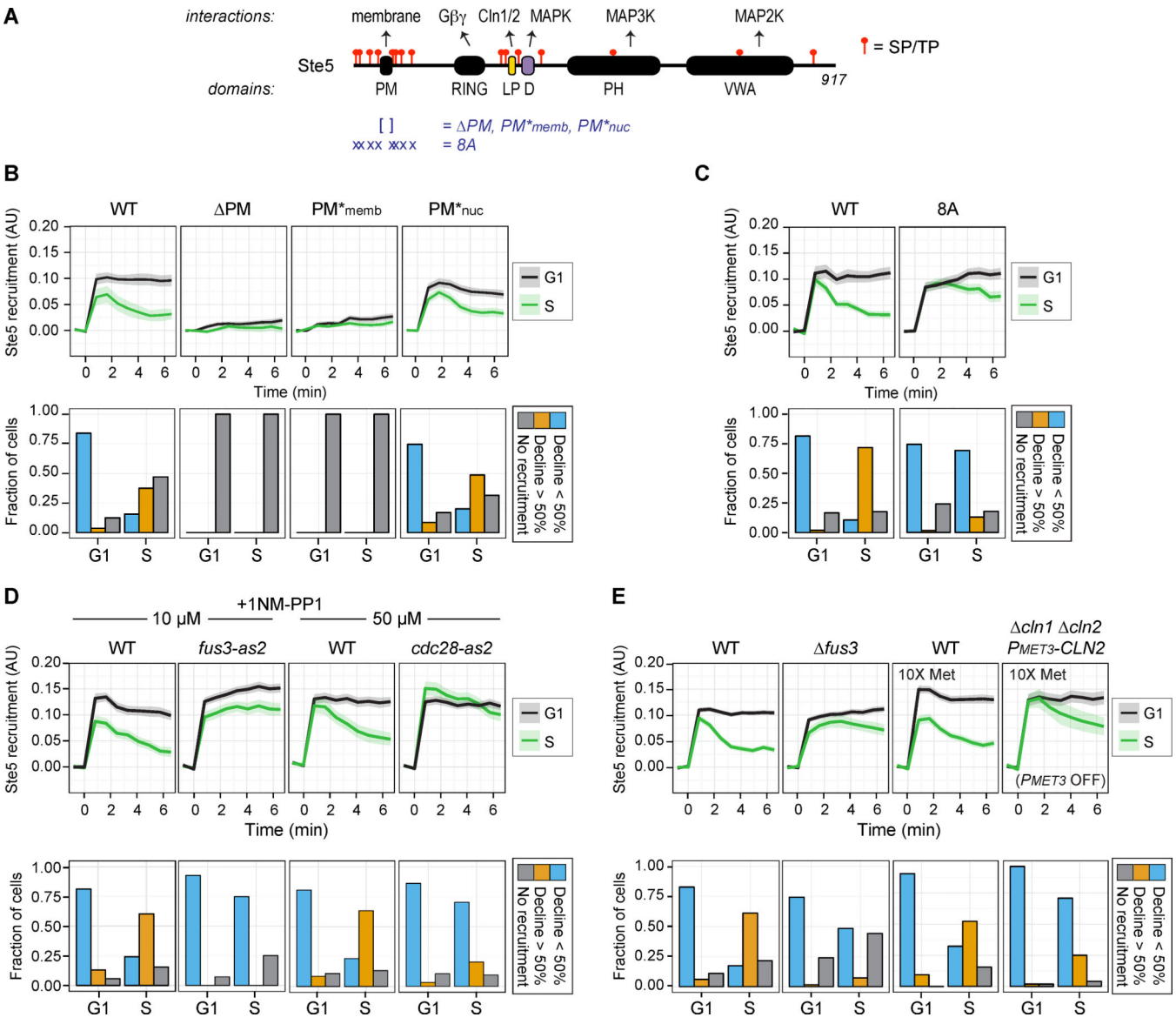

Figure 2. Both CDK and MAPK activities are required to regulate Ste5 recruitment

(A) Ste5 domain structure, interactions, and SP/TP phosphorylation motifs. *Below*, mutations tested in subsequent panels.

(B) Initial recruitment requires the PM domain. The ΔPM and PM*$_{memb}$ mutants are defective at membrane binding; PM*$_{nuc}$ is specifically defective in nuclear localization (Winters et al., 2005). Here, and in all similar charts elsewhere, plots of recruitment vs. time show the mean (dark line) ± 95%CI (shaded). Strains: MWY003, MWY012, MWY050, MWY015.

(C) The Ste5-8A mutation disrupts the S phase-specific decline. Strains: MWY003, MWY029

(D) S-phase decline requires both Fus3 and Cdc28 activity. Strains: VRY5013, VRY5090, MWY003, MWY090.

(E) Ste5 recruitment in cells lacking Fus3 (*Δfus3*) or the G1 cyclins Cln1 and Cln2 (*cln1Δ cln2Δ* P_{MET3}-*CLN2* cells, transferred to +Met medium 60 min. before the experiment). Also see Figure S2A-B. Strains: MWY003, VRY3839, MWY130.

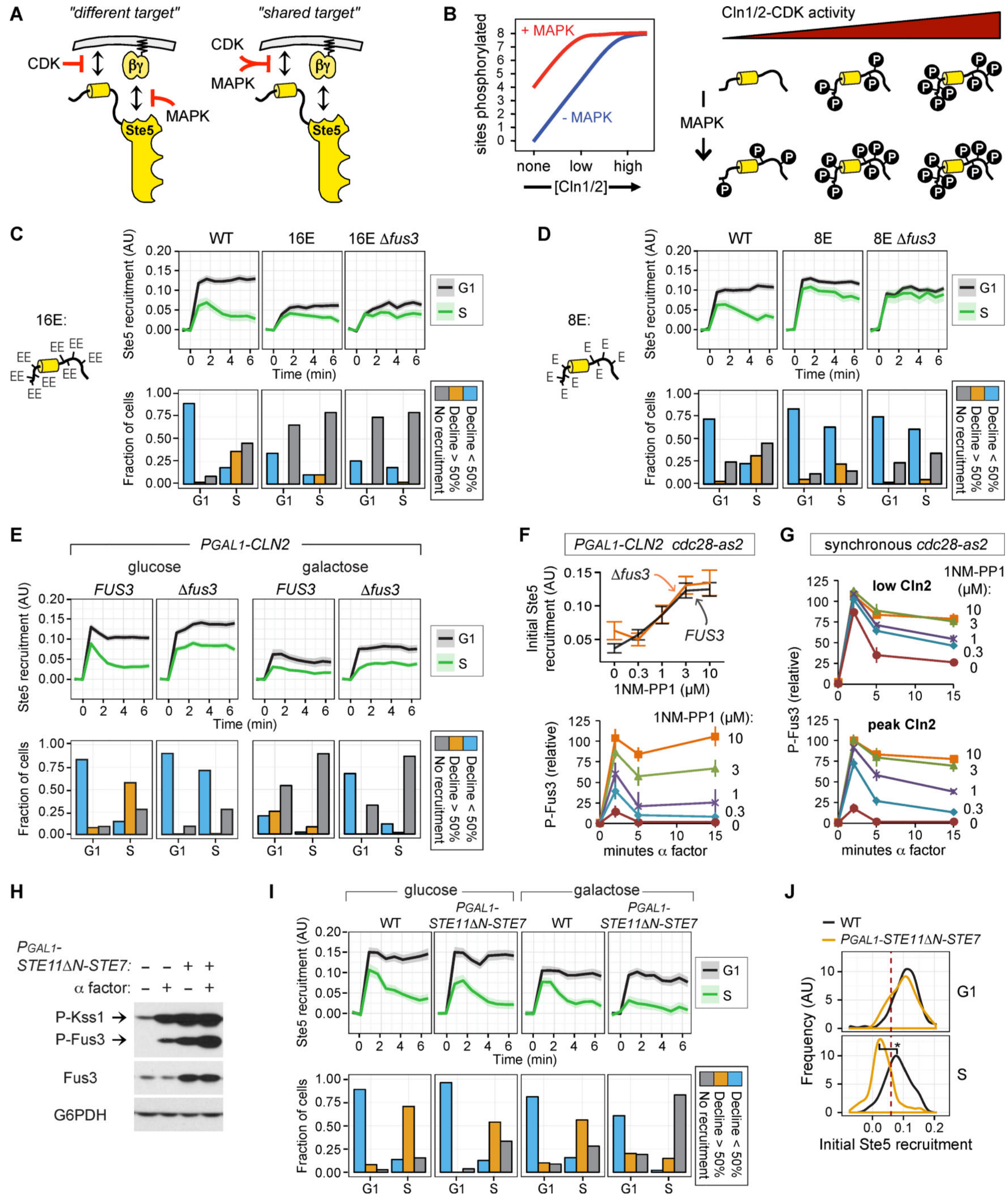

Figure 3. CDK and MAPK co-regulate the same target domain in Ste5

(A) Alternate models for collaborative regulation by CDK and MAPK.

(B) In the "shared target" model, the number of sites phosphorylated is a composite function of both Cln1/2-CDK and MAPK activity levels.

(C) For Ste5-16E, recruitment is blocked, and the role of Fus3 is bypassed. The 16E mutation replaces 8 SP/TP motifs with 8 EE motifs (see cartoon), which mimics constitutive phosphorylation at the 8 N-terminal sites. Strains: MWY003, MWY009, VRY5058.

(D) For Ste5-8E, initial recruitment is normal but decline behavior is disrupted. The 8E mutation replaces each of the 8 N-terminal sites with single E residues (see cartoon), which partly mimics phosphorylation while preventing further modification. Strains: MWY001, MWY052, VRY5755.

(E) Ste5 recruitment is blocked by induction of P_{GAL1}-*CLN2*. Strains: MWY136, VRY4095. The stronger block in S phase is likely because P_{GAL1}-*CLN2* is supplemented by *CLN1* and *CLN2* genes expressed from their native loci.

(F) Initial recruitment and Fus3 activation increase as CDK activity is reduced. Cln2-CDK activity was varied by inducing P_{GAL1}-*CLN2* expression in *cdc28-as2* cells, and then adding varying doses of 1NM-PP1. *Top*, initial recruitment (mean ± 95% CI); see Figure S3F-G for extended data. Strains: MWY136, VRY4095. *Bottom*, Fus3 activation (mean ± SEM; n = 3).

(G) Fus3 phosphorylation (mean ± SEM; n = 3) in *cdc28-as2* cells (MWY090) synchronized by α factor arrest and release. At times of peak or low Cln2 levels (45 or 75 min., respectively; see Figure S3G), cells were treated with 1NM-PP1 (5 min.) then re-stimulated with α factor.

(H) P_{GAL1}-*STE11ΔN-STE7* activates Fus3 without pheromone. Cells were induced with galactose (75 min.), then treated ± α factor (5 min.); note, prolonged pathway signaling activates *FUS3* gene expression, yielding elevated Fus3 protein levels in lanes on the right.

(I) Pre-activation of Fus3 by P_{GAL1}-*STE11ΔN-STE7* blocks initial Ste5 recruitment in S-phase cells. Strains: MWY003, MWY259.

(J) Histograms of initial recruitment in galactose-treated cells from panel I. Dashed line marks the “no recruitment” threshold. Asterisk, $p = 7 \times 10^{-8}$.

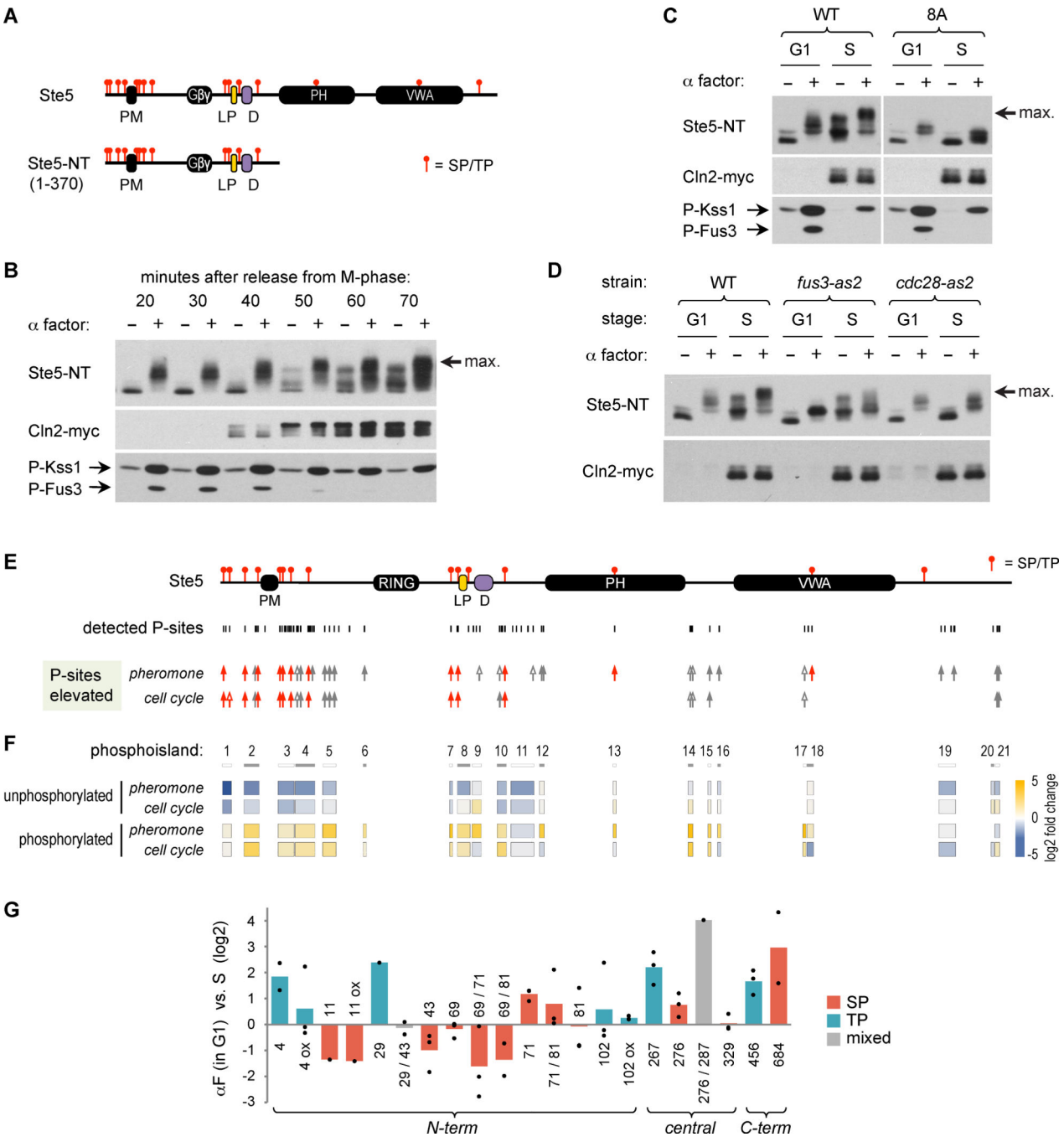

Figure 4. Collaborative phosphorylation and mass spectrometry analysis

(A) Diagram of Ste5 and the Ste5-NT fragment used in mobility shift assays of phosphorylation.

(B) Cultures of *cdc15-2* cells (MWY198) harboring HA-tagged Ste5-NT were synchronized by M-phase arrest and release. At times shown, cells were incubated ± α factor for 5 min. Ste5- NT mobility, Cln2-myc levels, and MAPK phosphorylation were assayed by immunoblotting. The arrow marks maximally shifted forms that require both Cln2 and pheromone.

(C) The Ste5-8A mutation reduces phosphorylation by pheromone or cell cycle alone, and prevents the maximal shift in the combined case. Note, the 8A mutation is present only in the HA-tagged Ste5-NT fragment, not in full-length Ste5 that mediates pheromone response.
(D) Strains (MWY198, MWY325, MWY333) were synchronized and then treated briefly with 1NM-PP1 prior to incubation ± α factor. Note that Fus3 and Cdc28 mediate effects of α factor and cell cycle, respectively, and that both are required for the maximal shift. Pheromone also has a Fus3-independent effect; see Figure S4F and Figure S6C.
(E) Summary of mass spectrometry data on Ste5 phosphorylation in vivo. For details, see Table S2 and Figure S5. To assess pheromone effects, G1 cells were compared ± α factor. To assess cell cycle effects, untreated G1- and S-phase cells were compared. Tick marks denote all detected phosphorylated sites, which include some that could not be quantified. Arrows show sites with elevated phosphorylation (> 1.5x): red, SP/TP sites; grey, other sites; unfilled arrowheads, increases detected in only 1 of 3 experiments.
(F) Heat map plots show changes in the abundance of unphosphorylated and phosphorylated peptides, grouped into phosphoislands (see Method Details). Large reductions in unphosphorylated peptides indicate extensively phosphorylated regions.
(G) Ratio of phosphorylation at SP/TP sites after pheromone treatment vs. cell cycle entry. Bars, mean values; black dots, values from individual biological replicates. “ox”: oxidized peptide generated during sample preparation.

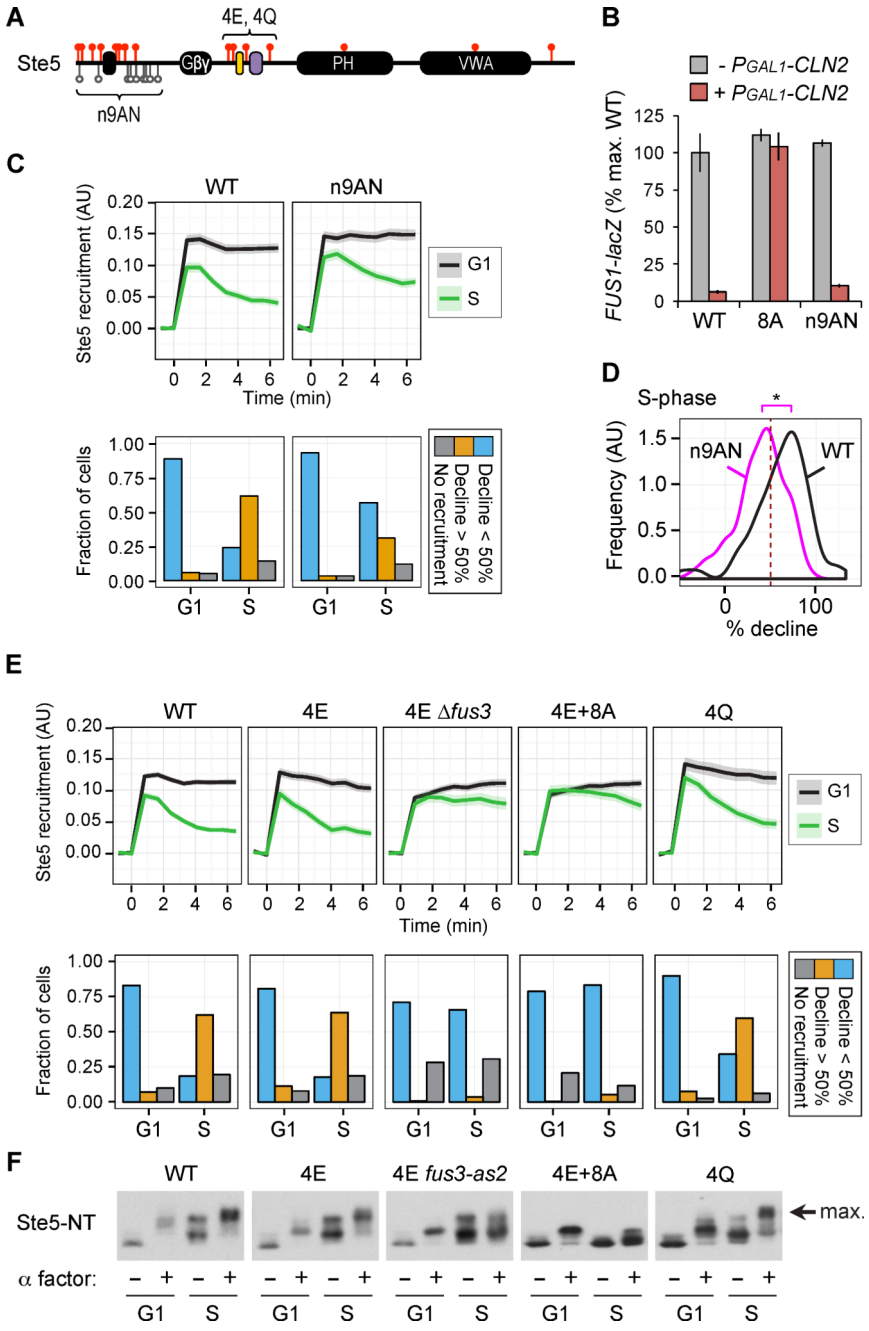

Figure 5. Role of pheromone and Fus3 is independent of the four central SP/TP sites

(A) Diagram of phosphorylation sites studied below.

(B) The Ste5-n9AN mutation does not prevent signaling from being blocked by P_{GAL1}-*CLN2*. Bars (mean ± SD; n = 3) measure a pheromone-inducible transcription reporter, *FUS1-lacZ*.

(C) The Ste5-n9AN mutant shows a partial defect in S-phase decline behavior. Strains: MWY003, MWY336.

(D) Histogram of declines in S-phase cells from panel C. Note that the Ste5-n9AN mutant is shifted to lower decline. Asterisk, $p = 4 \times 10^{-8}$. Dashed line marks the 50% decline threshold used in bar graphs of panel C. Strains: MWY003, MWY336.

(E) Recruitment of Ste5 with mutations (4E, 4Q) at the 4 central SP/TP sites, thought to be Fus3 targets. The 4E mutant was also analyzed in *fus3Δ* cells and combined with mutations at the 8 N-terminal sites (4E+8A). Strains: MWY003, MWY057, VRY3841, MWY160, MWY353.

(F) Ste5-NT phosphorylation results for mutants in the corresponding panel above. Note that achieving the maximal shift here correlates with the S-phase decline behavior above.

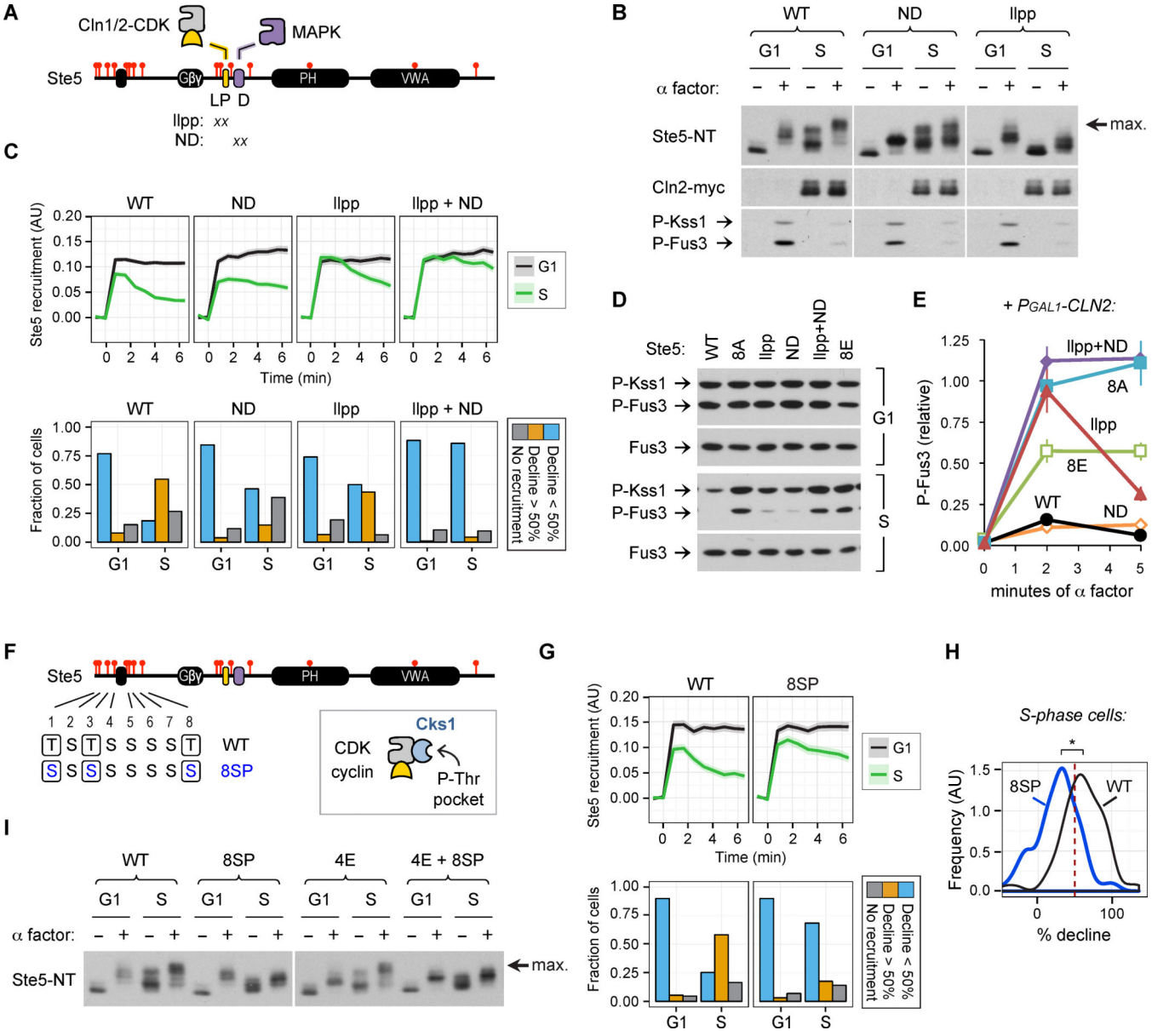

Figure 6. Regulatory roles for kinase docking motifs and phospho-Thr residues

(A) Docking motifs for Cln1/2 (LP motif) and Fus3 (D motif), and their mutations (llpp or ND).

(B) Mutations in LP and D motifs reveal that maximal Ste5-NT phosphorylation requires docking of the CDK and MAPK. Note, mutations are present only in the HA-tagged Ste5-NT fragment, and not in the endogenous Ste5.

(C) Recruitment results for Ste5 with mutations in the LP, D, or both motifs. Strains: MWY003, MWY153, MWY040, MWY169.

(D) Signaling by Ste5 mutants in G1 vs. S phase. Cultures were synchronized by α factor arrest and release. After 15 min. (G1) or 45 min. (S), aliquots were briefly re-stimulated with α factor. Strains: MWY001, MWY006, MWY355, MWY038, MWY168, MWY052.

(E) Early Fus3 phosphorylation kinetics (mean ± SEM, n = 6) in Ste5 mutant strains expressing P_{GAL1}-*CLN2* (pPP3376). Strains, as in panel D.
(F) The 8SP mutant has three TP sites replaced with SP. Inset: cyclin-CDK complexes include a Cks1 subunit with a phospho-threonine (P-Thr) binding pocket.
(G) Ste5-8SP shows a partial defect in the S-phase decline behavior. Strains: MWY003, MWY278.
(H) Histogram of Ste5 declines in S-phase cells from panel G. Asterisk, $p = 1 \times 10^{-10}$.
(I) Cell cycle-dependent mobility shift of Ste5-NT is altered by the 8SP mutation, both alone and in the context of the 4E mutation (which eliminates remaining SP/TP sites).

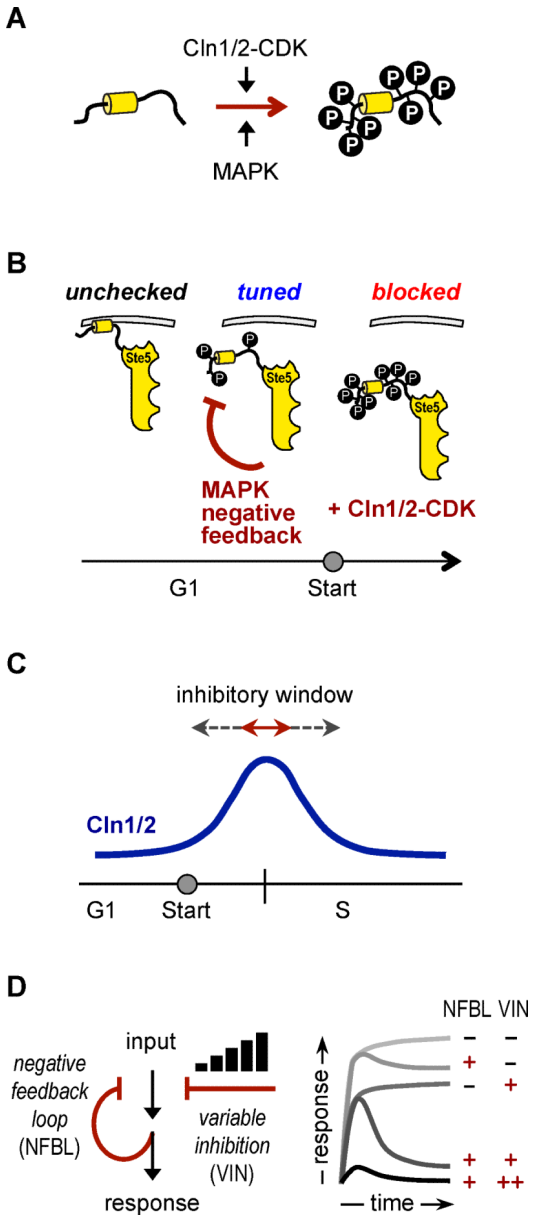

Figure 7. Models for collaborative regulation of Ste5 by CDK and MAPK inputs

(A) CDK and MAPK jointly contribute to full multi-site phosphorylation.

(B) Cell cycle regulation and negative feedback operate via same phosphorylation sites. Regulatory consequences can range from mildly tuned to strongly blocked, depending on cell cycle stage.

(C) Cooperative regulation can broaden the inhibitory window by allowing strong inhibition of Ste5 at sub-peak levels of Cln1/2.

(D) A generalized signaling circuit combining negative feedback with variable inhibition (left) can yield a range of response behaviors (right).